Antigen experience history directs distinct functional states of CD8+ CAR T cells during the anti-leukemia response

Terry Fry (TERRY.FRY@CUANSCHUTZ.EDU)
University of Colorado Anschutz Medical Campus
Kole DeGolier
University of Colorado Anschutz Medical Campus https://orcid.org/0000-0002-4144-7277
Etienne Danis
University of Colorado Anschutz Medical Campus
Marc D'Antonio
University of Colorado School
Jennifer Cimons
University of Colorado Anschutz Medical Campus https://orcid.org/0000-0002-8111-8697
Michael Yarnell
University of Colorado Anschutz Medical Campus https://orcid.org/0000-0002-4557-7255
Ross Kedl
University of Colorado Anschutz Medical Campus https://orcid.org/0000-0002-9065-7895
Mark kohler
University of Colorado School of Medicine
James Scott-Browne
National Jewish Health

Article

Keywords:

Posted Date: December 21st, 2023

DOI: https://doi.org/10.21203/rs.3.rs-3712137/v1

Additional Declarations: Yes there is potential Competing Interest. Patent applicant (whether author or institution): University of Colorado Anschutz Medical Campus Name of inventor(s): Kole R DeGolier,

James P Scott-Browne, Terry J Fry Application number: U.S. Provisional Application No. 63/595,612 Status of application: Pending Aspect covered: Methods of enhancing potency of engineered immune cells via Runx2 modulation

Antigen experience history directs distinct functional states of CD8+ CAR T cells during the anti-leukemia response

Kole R. DeGolier[1,2], Etienne Danis[3], Marc D'Antonio[1], Jennifer Cimons[1,2], Michael Yarnell[2,4], Ross M. Kedl[1], M. Eric Kohler[1,2,4], James P. Scott-Browne[1,5], Terry J. Fry[1,2,4]

[1] Department of Immunology, University of Colorado Anschutz Medical Campus; Aurora, CO, USA
[2]Department of Pediatrics, University of Colorado Anschutz Medical Campus; Aurora, CO, USA
[3]Biostatistics and Bioinformatics Shared Resource, University of Colorado Cancer Center, University of Colorado Anschutz Medical Campus; Aurora, CO, USA
[4]Center for Cancer and Blood Disorders, Children's Hospital Colorado; Aurora, CO, USA
[5]Department of Immunology and Genomic Medicine, National Jewish Health, Denver, CO, USA

Corresponding author:

Terry J Fry, MD
University of Colorado Anschutz Medical Campus and Children's Hospital Colorado
13123 E 16th Avenue
Aurora, Colorado 80045
Phone: 303.724.7293
Email: terry.fry@cuanschutz.edu

Running title: Antigen experience history directs distinct functional states of CD8+ CAR T cells during the anti-leukemia response

Nature Immunology

Abstract word count: 200 (200)
Manuscript word count: 4147 (4300)
Tables and Figure count: 6 figures, no tables (5-6 modest length (1/4 page))
Extended Data: 9 figures, no tables (10)
References: 39 (50)
Methods References: 12

ABSTRACT

Chimeric antigen receptor T cells are an effective therapy for B-lineage malignancies. However, many patients relapse and this therapeutic has yet to show strong efficacy in other hematologic or solid tumors. One opportunity for improvement lies in the ability to generate T cells with desirable functional characteristics. Here, we dissect the biology of CD8+ CAR T cells (CAR8) by controlling whether the T cell has encountered cognate TCR antigen prior to CAR generation. We find that prior antigen experience influences multiple aspects of *in vitro* and *in vivo* CAR8 functionality, resulting in superior effector function and leukemia clearance in the setting of limiting target antigen density compared to antigen-inexperienced T cells. However, this comes at the expense of inferior proliferative capacity, susceptibility to phenotypic exhaustion and dysfunction, and inability to clear wildtype leukemia in the setting of limiting CAR+ cell dose. Epigenomic and transcriptomic comparisons of these cell populations identified overexpression of the Runx2 transcription factor as a novel strategy to enhance CAR8 function, with a differential impact depending on prior cell state. Collectively, our data demonstrate that prior antigen experience determines functional attributes of a CAR T cell, as well as amenability to functional enhancement by transcription factor modulation.

Adoptive transfer of T cells expressing chimeric antigen receptors (CARs) has been highly successful for treating relapsed and treatment-refractory B-lineage hematologic malignancies. However, many patients do not achieve complete remission, or relapse. Poor response or lack of remission durability results from cancer cell resistance or suboptimal CAR T cell function[1]. Thus, further studies into the immunobiology of these engineered cells are warranted to enhance remissions and expand therapeutic potential to other hematologic and solid tumors. CAR T cells are commonly generated from a heterogeneous population of peripheral blood T cells that varies between patients, likely impacting the quality of a CAR T cell product[2]. Although it has been difficult to track cell fate through the manufacturing process and into patients, previous reports have shown differential function of CAR T cell products generated from memory versus naïve T cells sorted by surface marker phenotypes, which are not always an accurate representation of cellular differentiation state[2,3,4]. Emerging studies have demonstrated that phenotypic, transcriptomic and epigenomic attributes of the CAR product can influence patient outcomes[5].

During acute infections, naïve CD8+ T cells become activated through the T cell antigen receptor (TCR) by antigen presenting cells displaying cognate antigen and co-stimulatory ligands, and subsequently enter a highly regulated differentiation trajectory. A phase of rapid expansion and differentiation into effector cells is followed by contraction and formation of long-lived memory cells that rapidly respond to future exposures. However, if the pathogen is not cleared, antigen-specific T cell populations will receive recurring antigen stimulation. In this setting, rather than forming functional memory, T cells differentiate down a trajectory characterized by progressive dysfunction, preventing immune-mediated pathology, but simultaneously failing to clear the challenge. A growing body of work demonstrates that these differentiation trajectories (and resulting functional characteristics imbued on T cells) are controlled epigenetically in traditional T cell responses to viral infections and tumors. These programs are defined by progressive changes to the epigenome, associated with DNA methylation and histone modifications which are driven by a variety of transcription factors (TFs) and modulated by antigen receptor signaling[6]. These molecular modifications alter chromatin accessibility and transcriptional profiles which characterize cellular differentiation state and functional capacity. Epigenetic modulation of T cells via stimulation through the physiologic TCR has a well-established role in impacting the differentiation program and functional capacity of a pool of antigen-experienced T cells[7]. Emerging data also highlight the importance of epigenetic remodeling in CAR T cell responses to tumors[5].

Here, we carefully examine and compare the biology of CAR-transduced CD8+ T cells that differ as to whether cognate antigen has been encountered through the TCR prior to transduction with a CAR. We hypothesize that 1) T cells exhibit functional characteristics after CAR transduction that are dictated by prior antigen experience via the TCR 2)the functional characteristics of CAR8 derived from naïve or memory cells are the result of epigenetic attributes maintained through CAR transduction and reinfusion, and that 3) TF modulation as a modality to enhance CAR8 function may be dependent on the epigenetic and transcriptomic contexts determined by prior antigen experience status. Prior work has shown dose-dependent effects in the anti-tumor responses of adoptively-transferred T cells[2] and CAR T cells have been shown to elicit poor responses to tumors with low antigen density[1, 8, 9, 10]. Using limiting target antigen density or limiting T cell dose as stressors, we show that prior T cell antigen experience influences *in vitro* and *in vivo* functional characteristics of T cells stimulated through a CAR. Comparison of the epigenetic and transcriptomic states of CAR8 stratified by prior antigen-experience

status revealed differential chromatin accessibility and transcriptional programming. We pinpoint divergent RUNX2 activity within the two populations as a potential driver of differential function and show that ectopic expression of RUNX2 enhances the anti-leukemia response and mediates exhaustion resistance in CAR T cells in a manner dependent on prior T cell antigen experience status.

RESULTS

T cell antigen experience prior to transduction with a CAR directs *in vitro* proliferative and effector capacities of CD8+ CAR T cells.

Memory T cells demonstrate superior antigen sensitivity compared to naïve T cells in some contexts[11,12]. Thus, we hypothesized that CAR T cells derived from a memory T cell population would exhibit enhanced responsiveness to low antigen density leukemias compared to naïve-derived CAR T cells. T cells expressing a CAR containing an anti-mouse CD19 scFv incorporating a FLAG sequence and a CD28 costimulatory domain fused to mouse CD3zeta, followed by a 2A sequence and a truncated EGFR [13] (Figure S1A) were used to target a murine leukemia driven by the E2A-PBX1 fusion protein (E2A-PBX)[14, 15, 16]. FLAG-specific antibody detection of the CAR correlated strongly with EGFR expression, allowing for use of EGFR as a marker for long term tracking of CAR+ cells *in vivo* (Figure S1B). We expanded this model by generating a set of clones of E2A-PBX which express differing CD19 densities (Figure 1A, S1C). Memory OT-I T cells generated using a well-characterized ovalbumin vaccination model [17, 18, 19] (Figure 1B). were used to produce memory-derived CD8+ CAR T cells ($CAR8_{MD}$) for comparison to naïve-derived CD8+ OT-I CAR T cells ($CAR8_{ND}$). As no difference was seen in leukemia control by memory or naïve-derived control T cells (Figure S1D), we used naïve-derived (EGFR8) in all subsequent experiments. A functional duality began to emerge upon *in vitro* testing. As predicted, a greater proportion of $CAR8_{MD}$ cells had a polyfunctional effector profile, producing both TNFa and IFNg, or degranulating (as measured by CD107a), most pronounced in response to low target antigen (Figure 1C-H; S1E-G). Interestingly, while the proportion of IFNg+ cells was greater in $CAR8_{MD}$, the proportion of TNFa+ cells was slightly increased in $CAR8_{ND}$, suggesting a predisposition toward either IFNg or TNFa (Figure 1C & F). However, $CAR8_{ND}$ outperformed $CAR8_{MD}$ in cell cycle entry (Ki67 expression; Figure 1I, S1H) and extended proliferative capacity (Figure 1J, S1I) across antigen densities. To compare polyclonal antigen-experienced and naïve T cells more analogous to human CAR T cells, we generated pathogen-elicited polyclonal T cells by infecting WT C57BL/6 mice with the common acute viral infection model LCMV-Armstrong. Memory (CD8+/CD44+/$CD49d^{Hi}$) and naïve (CD8+/CD44-/$CD49d^{Lo}$/CD62L+) T cell populations were FACS-sorted from the same mice 28 days after LCMV infection and used for CAR T cell manufacturing (Figure S2A). Polyclonal pathogen-elicited T cells behaved similarly *in vitro* to memory and naïve OT-I cells: $CAR8_{MD}$ demonstrated superior effector function (increased proportions of cells producing IFNg) and $CAR8_{ND}$ demonstrated superior proliferative capacity (Figure S2B-E). Thus, CD8+ T cell antigen experience prior to transduction with a CAR promotes effector functions at the expense of proliferative capacity.

Treatment of leukemia-bearing mice with a high CAR+ cell dose reveals enhanced cytotoxic profile and clearance of antigen-low leukemia by memory-derived CAR8.

Given the opposing functional profiles of naïve and memory-derived CAR8, we next compared the ability of these two populations to mediate tumor clearance *in vivo*. Mice were engrafted with WT (35,000 antigens per cell), $CD19^{Lo}$ (10,000 antigens per cell) or $CD19^{Neg}$ leukemia followed 3 days later by a dose of 1e6 CAR T cells. The $CD19^{Lo}$ clone antigen density was chosen based on differential *in vitro* responses and, although higher than antigen density reported for CAR relapses post-CD22 CAR treatment[9], is consistent with the drop-off in CAR sensitivity against other antigens[8, 10]. *Rag1*-deficient hosts enabled CAR T cell expansion without irradiation and limited CAR T cell antigen exposure to CD19 densities expressed on leukemia rather than endogenous B cells. While we did not observe differences in proportions of CAR T cells in the marrow at peak expansion on day 4 (Figure 2A), post-contraction (day 11) $CAR8_{ND}$ had increased proportions and total counts of CAR T cells in mice bearing WT and $CD19^{Lo}$ leukemia (Figure 2B-C, Figure S3A-B). Both CAR groups mediated robust clearance of WT leukemia by day 11. Although there was no significant difference in clearance of $CD19^{Lo}$ leukemia, 4/10 mice treated by $CAR8_{ND}$ had detectable leukemia at >15% of live bone marrow cells while all 10 mice treated with $CAR8_{MD}$ had minimal leukemic burdens (<5%) (Figure 2D). We next tested whether the enhanced clearance of $CD19^{Lo}$ leukemia was associated with maintenance of the superior cytotoxic capacity of $CAR8_{MD}$ observed *in vitro*. Upon *ex vivo* restimulation of CAR8 in the bone marrow, we found that, while IFNg production was highly variable, GZMB production was markedly greater in $CAR8_{MD}$ (Figure 2E-F). $CAR8_{MD}$ had significantly higher proportions of cells falling into short-lived effector cell (SLEC, IL7Ra-/KLRG1+) and effector memory precursor (EMP, CD27+/CD62L-) phenotypes, fewer cells in the central memory precursor phenotype (CMP, CD27+/CD62L+), and no change in memory precursor effector cell (MPEC, IL7Ra+/KLRG1-) populations (Figure S4B-E). Additionally, early expression of effector-associated TFs IRF4, T-bet and EOMES was greater in $CAR8_{MD}$ (Figure 2G-I). Finally, while mice bearing WT high-antigen leukemia showed no survival difference after treatment with $CAR8_{MD}$ versus $CAR8_{ND}$, mice bearing $CD19^{Lo}$ leukemia treated with $CAR8_{MD}$ showed a significant survival benefit, with 20% of mice surviving to the 80 day experimental endpoint (Figure 2J). Together, these data show that $CAR8_{MD}$ mediate superior clearance of $CD19^{Lo}$ leukemia relative to $CAR8_{ND,}$ associated with maintenance of effector function and expression of effector-associated markers.

Treatment of leukemia-bearing mice with a low CAR+ cell dose reveals enhanced proliferative capacity and clearance of WT leukemia by naïve-derived CAR8.

We next hypothesized that the benefit of enhanced proliferative capacity of naïve-derived CAR8 would emerge at a lower CAR+ cell dose (3e5). As anticipated, $CAR8_{ND}$ expanded to significantly higher numbers in the bone marrow by day 4 regardless of leukemia antigen density, mirroring *in vitro* proliferative assays (Figure 3A-B, S3C, 1I-J). While $CAR8_{ND}$ mediated enhanced clearance and survival in mice bearing WT leukemia, there was no improvement in leukemia clearance or survival of mice bearing $CD19^{Lo}$ leukemia (Figure 3C, 3I, S3D), potentially due to reduced potency. Indeed, *ex vivo* IFNg production was greater in $CAR8_{MD}$, although there was no difference in GZMB production or expression of IRF4, T-bet or EOMES (Figure 3D-H). $CAR8_{MD}$ consistently demonstrated significantly higher proportions of SLECs at the early timepoint consistent with high CAR doses, but these differences disappeared by day 11 and no differences were seen in the MPEC population (Figure S5A,B). While EMP and CMP patterns mimicked high dose experiments, the differences were much less

pronounced, indicating that naïve-derived cells largely became more "effector-like" with greater proliferative drive (Figure S5C,D), consistent with effector-polarization in the setting of low numbers of antigen-specific precursor populations[20, 21]. However, these changes, combined with the strong expansion, did not mediate survival benefit against $CD19^{Lo}$ leukemia (Figure 3I). Finally, we predicted that at this lower cell dose, T cell dysfunction could emerge. Indeed, $CAR8_{MD}$ expressed higher levels of exhaustion-associated markers against WT leukemia with failure of $CAR8_{MD}$ to control leukemia (Figure S5E-F, I-J). Interestingly, we found that $CD19^{Lo}$ leukemia drove similar proportions of exhaustion phenotypes in both CAR8 populations, demonstrating that chronic, uncleared antigen exposure, even at low antigen density, can drive dysfunction (Figure S5G-H, K-L). These findings highlight the importance of proliferative capacity and resistance to dysfunction afforded by $CAR8_{ND}$ at limiting cell dose.

Epigenetic profiling of naïve and memory-derived CAR8 shows differential chromatin accessibility at binding sites for bZIP, Tcf, Runx and other TF families.

We predicted that functional traits were a product of distinct epigenetic states, given that functional distinctions of naïve and memory-derived CAR8 were dictated by status prior to CAR transduction. To test this, we performed bulk ATAC-seq on naïve and memory-derived cells at three timepoints: *ex vivo* prior to CAR transduction (Day -5, "PreCAR"), *in vitro* after CAR transduction (Day 0, "PostCAR"), and after reinfusion into mice bearing $CD19^{Lo}$ leukemia (Day 4, "Tumor") (Figure 4A). Comparison of experimental replicates showed tight concordance of chromatin accessibility at each condition and timepoint (Figure S6A). Broadly, the data showed several thousand differentially accessible regions between either cell type compared to itself across timepoints, and between naïve and memory-derived cells at each timepoint (Figure S6B). We found predictable patterns of ATAC-seq signal at genetic loci involved in T cell activation or effector function, including higher accessibility in $CAR8_{MD}$ at *Gzmb*, *Gzmc*, and the *Pdcd1* loci encoding for the PD1 protein. Concurrently, we found greater accessibility in $CAR8_{ND}$ at the *Tcf7* loci encoding TCF1, a TF important for maintaining self-renewal capacity (Figure 4B).

We used ChromVAR[22], to associate these changes in chromatin accessibility to previously defined datasets and potential TF activities. Based on relative chromatin accessibility at regions that were differentially accessible in a published comparison of effector and memory CD8+ T cells after acute viral infection with LCMV-Armstrong[23], memory-derived CAR8 acquired effector-associated changes in chromatin accessibility during CAR generation in culture that were maintained after transfer into tumor bearing mice. CAR8 generated from memory T cells also had reduced chromatin accessibility at features associated with memory T cells. By comparison, naïve-derived CAR8 maintained chromatin accessibility patterns at regions associated with memory T cells and showed minimal skewing toward an effector-like profile[23] (Figure 4C). To associate these changes with specific TF activities, we used ChromVAR to compare chromatin accessibility at regions containing DNA sequence motifs bound by different TFs (Figure 4D). Classifying this data using a kmeans clustering strategy, we found that there were distinct patterns of motif-associated chromatin accessibility between conditions and across each of the timepoints (Figure 4E). While motifs for bZIP and Irf family TFs broadly looked similar at the PreCAR timepoint, and became progressively enriched in memory cells, Tcf family motifs started similar and became enriched in naïve cells at the latter timepoints, while E2A family motifs started highly enriched in naïve and progressively

converged. Uniquely, motifs for Runx family members were always more accessible in memory-derived cells and did not converge or diverge (Figure 4D-E, S6C). Overall, these data show epigenetic features imprinted in the starting CD8+ T cell population are maintained through CAR engineering.

Prior antigen experience directs distinct transcriptomic patterns of naïve and memory-derived CAR8.

To test whether the epigenetic states of naïve and memory-derived CAR8 resulted in concurrent transcriptomic changes, we performed bulk RNA-seq at the same timepoints as for ATAC-seq (Figure 4A). We found predictable differential gene expression at each timepoint, with genes associated with self-renewal and proliferative capacity (*Lef1, Sell, Id3, Tcf7, Slamf6, Il7r)* upregulated in the naïve-derived cells and genes associated with effector capacity and activation (*Prf1, Ifng, Klrg1, Gzmb, Prdm1, Id2, Pdcd1, Tbx21)* upregulated in the memory-derived cells (Figure 5A). Gene set enrichment analysis (GSEA) showed progressive bias by normalized enrichment score (NES) toward effector-like in memory-derived CAR8, and toward memory-like in naïve-derived CAR8[24, 25, 26] (Figure 5B-C). Analysis with gene sets comparing memory and naïve T cells showed progressive decrease in the normalized enrichment score of memory or naïve-derived CAR8 toward the derivative cell population of each, suggesting the effector/memory gene set enrichment axis as the more accurate indicator of cell fate over time[24, 25] (Figure S7A). Looking at the top differentially-expressed TFs between the populations at the PreCAR timepoint, we found many expected hits, including *Bhlhe40*, *Klf4*, *Tbx21*, *Id2* and many bZIP family members (*Jun*, *JunB*, *Fos*, *Cebpb*) represented in the memory-derived group, while *Zeb1*, *Myb* and *Lef1*, encoding TFs associated with self-renewal, were upregulated in the naïve-derived cells[23, 27] (Figure S7D). Notably, among the Runx family, which showed uniquely stable differential motif accessibility between naïve and memory cells (Figure 4D), *Runx2* was among the most differentially expressed TF genes with marked overexpression in memory derived cells (Figure S7D). Ingenuity Pathway Analysis of global transcriptional profile implicated similar TF drivers[28](Figure S7B) with numerous distinct patterns of differential TF expression between memory and naïve-derived T cells. However, a very common pattern among ChromVAR-implicated TFs was high initial expression in memory cells at the PreCAR timepoint, followed by a convergence in expression between memory and naïve-derived CAR T cells at the PostCAR and Tumor timepoints, as seen with bZIP family members *Jun*, *Fos* and *Atf3*, along with the gene *Tbx21*, encoding canonical effector TF T-bet (Figure 5D). Among the Runx family, *Runx1* and *Runx3* gene expression tracked relatively closely between memory and naïve-derived cells at each timepoint, while *Runx2* followed the “high in memory, then converging” pattern which was commonly found among other TF families (Figure 5E). In summary, naïve and memory-derived T cells show differential gene expression and gene set association with self-renewal or memory-associated genes and activation or effector-associated genes, respectively. Many relevant TF genes show a pattern of high initial expression in memory cells at the PreCAR timepoint which converges between the cell derivations upon transduction with a CAR and reinfusion into tumor-bearing hosts.

RUNX2 overexpression boosts leukemia clearance, CAR T cell potency and CAR proportions in bone marrow.

To validate the epigenetic and transcriptomic data, we overexpressed two TFs from the ChromVAR-implicated bZIP family, BATF and c-Jun, both of which have been previously reported to impact CAR T cell function (Figure 6A-B)[29, 30, 31]. Although neither TF increased cytokine production or proliferation *in vitro* (Figure S8C-E), overexpression of either TF enhanced leukemia clearance by memory and naïve-derived CAR T cells (Figure 6C-D). There was no difference between BATF-CAR8 or JUN-CAR8 and control CAR8 in the PD1+ proportion (Figure S9C,E), co-expression of PD1 with markers of exhaustion (PD1+/CD39+ and PD1+/TOX+), or in the terminally exhausted Tcf1-/Tim3+ population (Figure S9D,F-H).

Due to the memory-like state of $CAR8_{ND}$, we anticipated that comparison of factors enriched in memory cells over naïve cells could reveal important drivers of memory cell function that were not fully induced in naïve cells during the synthetic engineering process. Given the unique profile of chromatin accessibility for Runx-family binding motifs coupled with the pattern of *Runx2* transcript expression which was high in PreCAR memory CD8+ T cells and then lost upon CAR transduction, we hypothesized that establishing RUNX2 expression in $CAR8_{ND}$ could enhance the existing memory-like profile of these T cells and boost T cell potency and anti-leukemia response. Murine RUNX2 was introduced into the pMSCV-IRES-eGFP (pMIG) backbone, containing a GFP reporter gene for long-term tracking of RUNX2-transduced T cell populations (RUNX2). Co-transduction of naïve CD8+ T cells with CAR-EGFR reporter and RUNX2-GFP reporter resulted in a large proportion of cells expressing both EGFR and GFP (Figure 6A). Upon intracellular staining for the RUNX2 protein, we found that the EGFR+ population in the RUNX2-transduced group showed approximately a 10-fold increase in RUNX2 expression relative to empty pMIG-transduced cells (Figure 6B). Co-culture of RUNX2-CAR8 and leukemia with a range of antigen densities revealed similar cytokine production and proliferation relative to pMIG-CAR8 (Figure 6C-D). To stress the ability of RUNX2-CAR8 to clear WT leukemia, we used an ultra-low CAR+ dose (1e5), against which both $CAR8_{ND}$ and $CAR8_{MD}$ exhibit markers of exhaustion and fail to control leukemia (Figure S7A-C). RUNX2 overexpression in $CAR8_{ND}$ strongly enhanced leukemia clearance and increased CAR proportions and absolute numbers in the marrow at 11 days post-CAR infusion (Figure 6E-F). While there was no difference in the PD1+ proportion, consistent with similar activation, mice treated with RUNX2-$CAR8_{ND}$ exhibited dramatically reduced proportion of PD1+/TOX+ cells, a lower proportion of PD1+/CD39+ cells and reduced proportions of TCF1-/TIM3+ cells, suggesting that RUNX2 overexpression counteracts the differentiation trajectory toward terminal exhaustion (Figure 6L, S9M-N,P)[27, 32]. $CAR8_{MD}$ showed less of an increase in RUNX2 following transduction with RUNX2-eGFP (Figure S7F) potentially due to higher RUNX2 at baseline (Figure 5E). Nonetheless, RUNX2-overexpression resulted in a significant reduction in the PD1+/CD39+ exhaustion phenotype of RUNX2-$CAR8_{MD}$ responding to WT leukemia and reduction in leukemia counts in marrow (Figure S9I) but no difference in other exhaustion phenotypes, CAR proportions or CAR counts (Figure 6K, S9K,L,O). We demonstrate that Runx2 overexpression in naïve-derived T cells enhances maintenance of CAR T cells in the marrow, boosts leukemia clearance and mediates a favorable exhaustion profile at a highly sub-curative CAR T cell dose with less impact in memory-derived CAR T cells, demonstrating that TF overexpression has a differential impact depending on starting T cell state.

DISCUSSION

Factors underlying tumor relapse after CAR T cell therapy are a central focus of study in the field of cell therapies for leukemia. Advances have been made in understanding and engineering solutions to prevent tumor cell escape via antigen modulation, T cell dysfunction, and poor T cell trafficking/persistence[1]. However, defining *in vitro* and *in vivo* functional strengths and cellular profiles associated with different starting T cell populations may be an opportunity to specifically identify approaches to arm CAR T cells to overcome different tumor escape modalities. Importantly, refining qualities of the starting cell population will likely be a large contributor to efficacy of cellular therapeutics derived from healthy allogeneic donors or induced pluripotent stem cells, or in the case of *in vivo* transduction platforms targeting genetic payloads to specific cell populations. Recent work has sought to use targeted modulation of TFs to enhance CAR T cell function or prevent dysfunction, with several publications focusing on the bZIP TF family, including forced expression of BATF and c-Jun, or genetic deletion of the Nr4a family of nuclear receptors[29, 30, 31, 33, 34]. However, the impact of modulation of the bZIP family has been variable. Therefore, we set out to characterize functional attributes programmed by prior T cell antigen experience, with the prediction that these would be tied to epigenetic traits. We anticipated that downstream modulation of TFs implicated by this framework might have divergent functional outcomes depending on starting cell population.

In this study, we use a syngeneic murine model with anti-mouse CD19 CAR T cells targeting murine pre-B cell leukemia enabling more natural T cell differentiation trajectories without xenogeneic TCR stimulation. We also used a well-defined vaccine model for precise control of the antigen experience history of CAR T cells with a clonotypic TCR, with confirmation in a polyclonal memory response. With limiting T cell dose or low target antigen density as “stressors,” we report that antigen experience dictates multiple functional outputs of CAR T cells. Memory-derived CAR T cells exhibited stronger cytotoxic function across target antigen densities, while naïve-derived CAR T cells show greater proliferative capacity and more rapid cell cycle entry. This was associated with enhanced activity against low-antigen density leukemia by memory derived CAR T cells and enhanced activity of naïve-derived cells at limiting cell dose, a setting that drove phenotypic exhaustion and dysfunction of memory-derived cells.

T cell differentiation is a product of epigenetic and transcriptomic state[23, 27] and while CAR T cells have been extensively profiled post-manufacturing, little work has been done to characterize effects of prior T cell state on post-transduction CAR T cell profiles[5]. We demonstrate that features of these states are maintained through CAR manufacturing and associate with differences in functional profiles. Specifically, we find significant differences in bZIP family transcription factors, which have been previously implicated in CAR T cell function[29, 30, 31]. BATF or JUN mediated enhanced leukemia clearance in our model independent of starting cell state, indicating that these TFs may derive most of their early *in vivo* activity via binding to NFAT-AP1 composite motifs, which show high accessibility in both cell types. Surprisingly, there was no difference in phenotypic exhaustion in BATF or JUN-overexpressing CAR T cells relative to control, indicating preservation of function in an exhausted state rather than prevention of exhaustion.

As a novel finding, we use epigenomic and transcriptomic assays and implicate modulation of Runx-family TFs, particularly Runx2, as having a likelihood for higher impact in naive-derived cells compared to memory. Ectopic RUNX2 expression in naïve-derived CAR T cells resulted in superior clearance of leukemia, higher proportions

of cells in the marrow, and reduced proportions of cells displaying terminally exhausted phenotypes relative to control. Our data suggest that RUNX2 overexpression, in contrast to overexpression of bZIP family members, can enhance functional potency of naïve-derived CD8+ CAR T cells while preventing entry into the exhaustion differentiation trajectory.

In addition to their activity as transcriptional activators, Runx family members have been shown to recruit chromatin remodeling factors to Runx binding sites to open these sites and allow for transcriptional activation. In other model systems, RUNX2 has been shown to interact with SWI/SNF complexes, histone acetyltransferases (MOZ, p300), histone deacetylases (HDAC3, HDAC4, HDAC6) and histone methyltransferases (SUV39H1), along with all three TET family enzymes, indicating a plausibility for the ability for RUNX2 to recruit enzymes which participate in chromatin remodeling at RUNX binding motifs[35, 36, 37, 38]. These features could help explain the contribution of RUNX2 overexpression to the enhanced functionality and exhaustion resistance of $CAR8_{ND}$ seen in our experiments. Additional studies will be necessary to fully elucidate the effects of RUNX2 in CAR T cells, and to confirm our findings in human CAR T cells. Nonetheless, using a model in which antigen history can be precisely controlled, we show that RUNX2 overexpression enhances *in vivo* CAR T cell function dependent on the starting T cell. Finally, we have generated a framework for the role of antigen experience on function of a CAR T cell in stress situations of limiting T cell dose or target antigen density and highlight the importance of considering this framework when assessing the impact of approaches to apply synthetic immunology to manipulate therapeutic immune effector cell functions.

METHODS

See Supplemental Material.

AUTHOR CONTRIBUTIONS

K.R.D. Conceptualized the studies, performed experiments and data analysis, and wrote the manuscript. E.D. Performed data analysis and provided expertise related to ATAC/RNA sequencing. M.D. Performed experiments. J.C. Conceptualized the studies and provided expertise related to the murine CAR and leukemia models. M.Y. Designed and generated DNA constructs. R.M.K. Provided expertise related to the vaccine model. M.E.K. Conceptualized the studies and provided expertise related to the murine CAR and leukemia models. J.P.S-B. Performed data analysis and provided expertise related to ATAC/RNA sequencing. T.J.F. Conceptualized, supervised and provided funding for the studies, and wrote the manuscript. All authors contributed to the article and approved the submitted version.

ACKNOWLEDGEMENTS

We thank Lillie Leach for laboratory management, Amanda Novak for animal colony management, Garrett Hedlund and Henry Chu at the CU Anschutz Clinical Immunology Flow Core for their assistance in cell sorting, the CU Cancer Center Genomics Shared Resource (RRID: SCR_021984) for their help with sequencing/genomics, and the CU Anschutz OLAR and the animal facility for their support. This work was funded in part by Department of Defense W81XWH-19-1-0196 and partly supported by the National Institutes of

Health P30CA046934 Bioinformatics and Biostatistics Shared Resource Core (RRID: SCR_021983). Some figures were created with BioRender.com.

SUPPLEMENTAL METHODS

Mouse Strains

B6.129S6-Rag2tm1Fwa Tg(TcraTcrb)1100Mjb ("OT-I," Model #: 2334-F) mice were obtained from Taconic Biosciences. B6.SJL-Ptprca Pepcb/BoyJ ("PepBoy," Strain #:002014), B6.129S7-Rag1tm1Mom/J ("*Rag1*$^{-/-}$," Strain #:002216), C57BL/6J mice ("B6," Strain #:000664) were obtained from The Jackson Laboratory. Female mice were used for all experiments with B6 background mice. All mice were bred and/or maintained in the animal facility at University of Colorado Anschutz Medical Campus. All experiments were performed in compliance with the study protocol approved by University of Colorado Anschutz Medical Campus Institutional Animal Care and Use Committee (IACUC).

Mouse CAR Constructs

The basic construction of the murine 1928z CAR was previously described[39]. The murine anti-CD19 scFv was Flag-tagged to enable CAR detection, and all ITAMs in the CD3zeta domain were kept intact. A truncated human EGFR reporter protein was incorporated following a 2A skip sequence to provide an additional method for detection of CAR-transduced cells[13]. The DNA was codon optimized, ordered from ThermoFisher GeneArt, and cloned into the MSCV-IRES-GFP backbone, a gift from Tannishtha Reya (Addgene plasmid # 20672 ; http://n2t.net/addgene:20672 ; RRID:Addgene_20672), using XhoI and ClaI enzyme sites. A control plasmid with just the truncated EGFR reporter in the MSCV backbone was generated using similar methods.

Cell lines and media

E2A-PBX pre-B cell acute lymphoblastic leukemia was developed in the laboratory as previously described[14, 15, 16]. Murine T cells and leukemia were cultured in Complete Mouse Media (CMM), consisting of RPMI 1640 medium (Gibco) with 10% heat-inactivated fetal calf serum (Omega Bio), 1% nonessential amino acids (Gibco), 1% sodium pyruvate (Gibco), 1% penicillin/streptomycin (Gibco), 1% L-glutamine (Gibco), 1% HEPES buffer (Gibco) and 50uM 2-mercaptoethanol (Sigma-Aldrich).

Mouse CAR Transduction

CAR transduction was performed as previously described[14, 15, 16]. Briefly, spleens from 6-10 week old donor mice were harvested and CD8+ T cells were isolated using EasySep Mouse CD8+ T cell Isolation Kit from STEMCell Technologies or bulk T cells were isolated using the Mouse CD3+ T Cell Enrichment Column Kit (R&D Biosciences, Cat No. MTCC-25). On day 1, T cells were activated on anti-CD3/anti-CD28 Mouse T cell Activator DynaBeads (Invitrogen) at a 1:1 cell:bead ratio and cultured at 1e6/mL in CMM in the presence of rhIL-2 (40IU/mL) and rhIL-7(10ng/mL) from R&D Systems. On days 2 and 3, retroviral supernatant was added to Retronectin-coated (Takara Biosciences) 6 well plates and spun at 2000xg and 32°C for 2-3 hours. Supernatant

was then removed and activated T cells were added to the wells at 1.67mL/well. On day 4, beads were removed and T cells were resuspended at 1e6/mL in fresh media with cytokines. CAR transduction was determined post-debeading by analyzing T cells by flow cytometry for a FLAG/EGFR double-positive population (or EGFR single-positive for control T cells), and T cells were used in assays or infused into mice on day 5 or 6.

Vaccine Model

The ovalbumin vaccine consists of 100ug whole ovalbumin protein (InvivoGen, Cat. code: vac-pova-100), 40ug anti-mouse CD40 (BioXCell, Catalog #BE0016-2) and 40ug Polyinosinic:polycytidylic acid [Poly (I:C)] (InvivoGen, Cat. code: tlrl-pic-5) per mouse, resuspended to 200uL total volume in PBS[17, 18, 19]. CD8+ T cells were isolated from naïve 6 to 8 week old OT-I mouse splenocytes using the Mouse CD3+ T Cell Enrichment Column Kit (R&D Biosciences, Cat No. MTCC-25). PepBoy mice were given 5e3 OT-I T cells retro-orbitally and concurrently vaccinated intravenously. 3-4 weeks later, spleens from 5-20 vaccinated mice were pooled and CD45.2+ OT-I memory T cells were isolated using the EasySep Mouse CD8+ T cell Isolation Kit, followed by column isolation using biotinylated anti-mouse CD45.2 (BioLegend, Cat # 109804), LS Columns (Miltenyi Biotec, Order No. 130-042-401), and anti-Biotin MicroBeads (Miltenyi Biotec, Order No. 130-090-485). Naïve T cells from 1-5 naïve OT-I donors were isolated in parallel. T cells were then activated and transduced as described for downstream experiments.

Generation of CD19^{Lo} E2A-PBX leukemia cell lines

The E2A-PBX murine leukemia was generated in our lab as previously described [14]. CD19 knockout leukemia was produced using CRISPR/Cas9. A previously-validated murine CD19-targeting sgRNA[15] from Integrated DNA Technologies was incubated with recombinant Cas9 from TakaraBio (Cat# 632641) to create an RNP complex. RNP was then electroporated into E2A-PBX using the Lonza 4D-Nucleofector X with nucleofector solution SG and pulse program CM-147. Electroporated cells were allowed to recover for 48 hours and then FACS-sorted twice to obtain a pure CD19 knockout cell line. This cell population was additionally single cell cloned to create a CD19 knockout single cell clone prior to transduction with murine CD19. A truncated/non-signaling murine CD19 was cloned into the pLV.SP146.gp91.GP91.cHS4 plasmid, a gift from Didier Trono (Addgene plasmid # 30480 ; http://n2t.net/addgene:30480 ; RRID:Addgene_30480). Backbones were generated with the hEF1a promoter (pLV.hEF1a.cHS4) or the hUbC promoter (pLV.hUbC.cHS4) from the pLenti6/UbC/mSlc7a1 plasmid, a gift from Shinya Yamanaka (Addgene plasmid # 17224 ; http://n2t.net/addgene:17224 ; RRID:Addgene_17224). VSV-G pseudotyped lentivirus was generated as described and E2A-PBX CD19KO underwent a single round of transduction using standard protocols, followed by single cell cloning to obtain clonally-derived lines expressing defined levels of CD19 target antigen.

Flow Cytometry

Flow cytometry analysis was performed using an LSR-Fortessa X-20 flow cytometer (BD Biosciences) and analyzed using FlowJo (BD Biosciences). Monoclonal antibodies used in staining are listed in the supplemental methods. Intracellular flow cytometry staining was performed using the TrueNuclear Transcription Factor Buffer

Set (BioLegend) for *ex vivo* staining of transcription factors, Cytofix/Cytoperm Fixation/Permeablization Kit (BD Biosciences) for intracellular cytokine staining, and Mouse Foxp3 Buffer Set (BD Biosciences) for intracellular staining of Ki67 and Runx2.

CD107a Degranulation, Intracellular Cytokine Staining (ICCS), Ki67 and CellTrace Dilution *In Vitro* Assays

In vitro assays were performed using a 1:1 effector to target cell ratio with 1e5 of each cell type in a 96-well round-bottom plate followed by analysis by flow cytometry at the indicated timepoints. Degranulation assays were performed by incubation for 4 hours in the presence of 2uM monensin and 1uL of CD107a antibody. ICCS was performed by incubation for 6 hours, with 1uM monensin and 2.5uM Brefeldin A added at 1 hour in. Ki67 was performed by incubation for 18 hours, followed by intracellular staining for Ki67. CellTrace dilution assays were performed by staining T cells with CellTrace Violet (Thermo Fisher Scientific) per manufacturer protocols followed by incubation with target cells for 72 hours.

LCMV infection and T cell isolation

6 week old female C57BL/6 mice were injected retro-orbitally with 2e5 PFU of LCMV-Armstrong. 4 weeks later, CD8+ T cells were isolated from 5 pooled spleens using the EasySep Mouse CD8+ T cell Isolation Kit from STEMCell Technologies and then FACS-sorted to obtain Memory (CD8+/CD44+/CD49d^{hi}) and Naïve (CD8+/CD44-/CD49d^{lo}/CD62L+) populations from the same mice. T cells were then transduced using the standard transduction protocol as described.

***In vivo* experiments in *Rag1*$^{-/-}$ hosts**

Experiments were carried out using a timeline previously optimized in the lab[14]. Briefly, *Rag1*$^{-/-}$ hosts were inoculated with 1e6 E2A-PBX by tail vein I.V. injection on day -3 followed by CAR T cells via retroorbital injection at either 1e5, 3e5 or 1e6 CAR+ cell dose on day 0. Bone marrow was harvested and analyzed by flow cytometry on day 4 or 11 post-CAR infusion, or mice were euthanized at humane endpoints for survival experiments. *Ex vivo* stimulation for cytokine production was performed using 1e6 E2A-PBX WT to stimulate approximately 1.5e6 whole bone marrow cells from each individual mouse, with pooled bone marrow from each n=5 experimental group stimulated by E2A-PBX CD19^{Neg} as a negative control. Cells were co-cultured for 6 hours, with 1uM monensin and 2.5uM Brefeldin A added at 1 hour in and then analyzed by flow for cytokine production.

Bulk ATAC and RNA sequencing experimental setup and workflows

OT-I CD8+ T cells were isolated from vaccinated or naïve donors and CARs were transduced into T cells as described above. CAR8 *Rag1*$^{-/-}$ hosts were inoculated with 1e6 E2A-PBX CD19^{10,000} followed by 1e6 CAR8$_{MD}$ or CAR8$_{ND}$ on the timeline described above. At day 4 post-CAR infusion, bone marrow from 10 mice per CAR group was harvested and pooled. At each of 3 timepoints, CD8+ cells were isolated using the EasySep Mouse CD8+ T cell Isolation Kit from STEMCell Technologies and then FACS-sorted to obtain 50,000 cells per condition. ATAC-seq and RNA-seq were performed in triplicate on separate sorted aliquots of 50,000 cells at “Pre-CAR/Day -5” (*ex vivo,* directly after isolation of memory or naïve CD8+ T cells from donor mice), “Post-CAR/Day 0” (*in*

vitro, after CAR manufacturing) and "Tumor/Day 4" (*ex vivo*, after reinfusion into leukemia bearing mice). Experimental analyses were performed on the first technical replicate from 2 separate experimental replicates. For RNA-seq, cells were homogenized in QIAzol Lysis Reagent (Qiagen, Cat. No. 79306) and then frozen at -80C for processing within 2 weeks. Samples were thawed and processed using the miRNeasy Micro Kit (Qiagen, Mat. No. 1071023), with on-column DNase treatment (RNase-Free DNase Set, Qiagen, Cat. No. 79254), both according to manufacturer protocols. RNA purity, quantity and integrity was determined with NanoDrop (ThermoFisher Scientific) and TapeStation 4200 (Agilent) analysis prior to RNA-seq library preparation. The Universal Plus mRNA-Seq library preparation kit with NuQuant was used (Tecan) with an input of 200ng of total RNA to generate RNA-seq libraries. Paired-end sequencing reads of 150bp were generated on NovaSeq 6000 (Illumina) sequencer at a target depth of 40 million clusters/80 million paired-end reads per sample. Raw sequencing reads were de-multiplexed using bcl2fastq. For ATAC-seq, cells were immediately processed using the Omni-ATAC protocol as previously described[40]. Briefly, sorted cells were washed once in 1X PBS, lysed, washed once in Wash Buffer and then the transposition reaction was carried out at 32°C for 30 minutes on a thermomixer set to 1000 rpm. Transposed chromatin was then purified using the Zymo Clean and Concentrator 5 Kit (Zymo Research, Cat # D4013) using manufacturer protocols. DNA was then ran on PCR for 12 total cycles with matched barcoding primers[41]. PCR reactions were then size-selected using AMPure XP beads (Beckman Coulter Life Sciences, Product No: A63880) and checked for quality and size distribution using TapeStation 4200 with D5000 reagents (Agilent). Libraries were pooled at equimolar ratios for sequencing and paired-end sequencing reads of 150bp for the first replicate and 50bp for the second replicate were generated on NovaSeq 6000 (Illumina) sequencer at a target depth of 40 million clusters/80 million paired-end reads per sample. Raw sequencing reads for replicate 1 were shortened to match the read lengths for replicate 2 using trimmomatic function CROP. Raw sequencing reads were de-multiplexed using bcl2fastq.

RNA-seq Data Analysis

Quality of fastq files was accessed using FastQC (v.0.11.8) (http://www.bioinformatics.babraham.ac.uk/projects/fastqc), FastQ Screen (v.0.13.0)[42] and MultiQC (v.1.8)[43]. Illumina adapters and low-quality reads were filtered out using BBDuk (v. 38.87) (http://jgi.doe.gov/data-and-tools/bb-tools). Trimmed fastqc files were aligned to the mm10 murine reference genome and aligned counts per gene were quantified using STAR (v.2.7.9a) [44]. Differential gene expression analysis was performed using the DESeq2 package[45]. Pathway enrichment analysis was performed using GSEA (UC San Diego/Broad Institute)[26, 46], Metascape[47] for gene mapping and IPA (Qiagen)[28, 48]. Differential gene expression was plotted using GraphPad Prism or ggplot2 (R package). RNA-seq differential gene expression statistics were run using the DESeq2 R package, with filtering threshold at 10 with greater than 2-fold change and adjusted p value < 0.05.

ATAC-seq Data Analysis

Fastq files were used to map to the mm10 genome using the ENCODE ATAC-seq pipeline (https://www.encodeproject.org/atac-seq/), with default parameters, except bam files used for peak calling were randomly downsampled to a maximum of 50 million mapped reads. Peaks with a

MACS2(https://pypi.org/project/MACS2/) computed q value of less than 1e-6 and a signalValue of more than 4 in at least one replicate were merged with bedtools[49] function intersect and processed to uniform peaks with the functions getPeaks and resize from R package ChromVAR[22]. Reads overlapping peaks were enumerated with getCounts function from ChromVAR and normalized and log2-transformed with voom from R package limma[50]. Peaks with 3 or more normalized counts per million mapped reads at least one replicate were included to define a global peak set of 82,410 peaks. Pairwise Euclidean distances were computed between all samples using log2-transformed counts per million mapped reads among the global peak set. Differentially accessible peaks were identified in pairwise comparisons based on fdr adjusted p values of less than 0.01, fold change of at least 4 and with an average of 3 normalized counts per million mapped reads using R package limma. Motif associated variability in ATAC-seq signal was computed with R package ChromVAR. Genome-wide visualization of ATAC-seq coverage was computed with deeptools[51] function coveragebam, using manually computed scale factors based on the number of reads within the total peak set.

Statistics

Statistical tests for all experiments except sequencing analyses were performed using GraphPad Prism v9.0 for Macintosh (GraphPad Software). Comparisons between three groups were made with ordinary one-way ANOVA with Holm-Sidak's multiple comparisons test, Brown-Forsythe and Welch one-way ANOVA with Dunnett's T3 multiple comparisons test, or Kruskal-Wallis non-parametric test with Dunn's multiple comparisons test were used depending on variance in standard deviations. Two-way ANOVA or mixed effects analysis with Tukey's multiple comparisons test was used for *in vitro* experimental comparisons with multiple antigen densities and *in vivo* CAR expansion data. Two-tailed ordinary t test, Welch's t test or Mann-Whitney test were performed for comparisons with two groups depending on normality of distributions. For multiple comparisons of two groups, multiple unpaired t tests or multiple Welch's t tests, both with Holm-Sidak's multiple comparisons test, were performed when appropriate depending on variance in standard deviations. Log-rank (Mantel-Cox) test was used for survival curve comparisons. All data represented as mean +/- standard deviation. * $p<0.05$, ** $p<0.01$, *** $p<0.001$, **** $p<0.0001$. Technical and experimental replicates in each dataset are indicated in figure legends.

Data and Materials Availability

All data is readily available from authors upon request or accessible at Gene Expression Omnibus (**GEO Accession Number will be provided before paper acceptance**). All materials are either commercially available as described or available from authors upon request.

REFERENCES

1. Labanieh, L. & Mackall, C.L. CAR immune cells: design principles, resistance and the next generation. *Nature* **614**, 635-648 (2023).

2. Sommermeyer, D. *et al.* Chimeric antigen receptor-modified T cells derived from defined CD8+ and CD4+ subsets confer superior antitumor reactivity in vivo. *Leukemia* **30**, 492-500 (2016).

3. Qin, H. *et al.* CAR T cells targeting BAFF-R can overcome CD19 antigen loss in B cell malignancies. *Sci Transl Med* **11** (2019).

4. Aldoss, I. *et al.* Favorable Activity and Safety Profile of Memory-Enriched CD19-Targeted Chimeric Antigen Receptor T-Cell Therapy in Adults with High-Risk Relapsed/Refractory ALL. *Clin Cancer Res* **29**, 742-753 (2023).

5. Alvanou, M. *et al.* Empowering the Potential of CAR-T Cell Immunotherapies by Epigenetic Reprogramming. *Cancers (Basel)* **15** (2023).

6. Frias, A.B., Boi, S.K., Lan, X. & Youngblood, B. Epigenetic regulation of T cell adaptive immunity. *Immunol Rev* **300**, 9-21 (2021).

7. Wherry, E.J. & Kurachi, M. Molecular and cellular insights into T cell exhaustion. *Nat Rev Immunol* **15**, 486-499 (2015).

8. Heitzeneder, S. *et al.* GPC2-CAR T cells tuned for low antigen density mediate potent activity against neuroblastoma without toxicity. *Cancer Cell* **40**, 53-69.e59 (2022).

9. Fry, T.J. *et al.* CD22-targeted CAR T cells induce remission in B-ALL that is naive or resistant to CD19-targeted CAR immunotherapy. *Nat Med* **24**, 20-28 (2018).

10. Majzner, R.G. *et al.* Tuning the Antigen Density Requirement for CAR T-cell Activity. *Cancer Discov* **10**, 702-723 (2020).

11. Kumar, R. *et al.* Increased sensitivity of antigen-experienced T cells through the enrichment of oligomeric T cell receptor complexes. *Immunity* **35**, 375-387 (2011).

12. Mehlhop-Williams, E.R. & Bevan, M.J. Memory CD8+ T cells exhibit increased antigen threshold requirements for recall proliferation. *J Exp Med* **211**, 345-356 (2014).

13. Wang, X. *et al.* A transgene-encoded cell surface polypeptide for selection, in vivo tracking, and ablation of engineered cells. *Blood* **118**, 1255-1263 (2011).

14. Qin, H. *et al.* Murine pre-B-cell ALL induces T-cell dysfunction not fully reversed by introduction of a chimeric antigen receptor. *Blood* **132**, 1899-1910 (2018).

15. Jacoby, E. *et al.* CD19 CAR immune pressure induces B-precursor acute lymphoblastic leukaemia lineage switch exposing inherent leukaemic plasticity. *Nat Commun* **7**, 12320 (2016).

16. Yang, Y. *et al.* TCR engagement negatively affects CD8 but not CD4 CAR T cell expansion and leukemic clearance. *Sci Transl Med* **9** (2017).

17. Ivanova, D.L. *et al.* Vaccine adjuvant-elicited CD8(+) T cell immunity is co-dependent on T-bet and FOXO1. *Cell Rep* **42**, 112911 (2023).

18. Klarquist, J. *et al.* B cells promote CD8 T cell primary and memory responses to subunit vaccines. *Cell Rep* **36**, 109591 (2021).

19. Klarquist, J. *et al.* Clonal expansion of vaccine-elicited T cells is independent of aerobic glycolysis. *Sci Immunol* **3** (2018).

20. Badovinac, V.P., Haring, J.S. & Harty, J.T. Initial T cell receptor transgenic cell precursor frequency dictates critical aspects of the CD8(+) T cell response to infection. *Immunity* **26**, 827-841 (2007).

21. Marzo, A.L. *et al.* Initial T cell frequency dictates memory CD8+ T cell lineage commitment. *Nat Immunol* **6**, 793-799 (2005).

22. Schep, A.N., Wu, B., Buenrostro, J.D. & Greenleaf, W.J. chromVAR: inferring transcription-factor-associated accessibility from single-cell epigenomic data. *Nat Methods* **14**, 975-978 (2017).

23. Scott-Browne, J.P. *et al.* Dynamic Changes in Chromatin Accessibility Occur in CD8(+) T Cells Responding to Viral Infection. *Immunity* **45**, 1327-1340 (2016).

24. Wherry, E.J. *et al.* Molecular signature of CD8+ T cell exhaustion during chronic viral infection. *Immunity* **27**, 670-684 (2007).

25. Luckey, C.J. *et al.* Memory T and memory B cells share a transcriptional program of self-renewal with long-term hematopoietic stem cells. *Proc Natl Acad Sci U S A* **103**, 3304-3309 (2006).

26. Subramanian, A. *et al.* Gene set enrichment analysis: a knowledge-based approach for interpreting genome-wide expression profiles. *Proc Natl Acad Sci U S A* **102**, 15545-15550 (2005).

27. Giles, J.R. *et al.* Human epigenetic and transcriptional T cell differentiation atlas for identifying functional T cell-specific enhancers. *Immunity* **55**, 557-574.e557 (2022).

28. Krämer, A., Green, J., Pollard, J., Jr. & Tugendreich, S. Causal analysis approaches in Ingenuity Pathway Analysis. *Bioinformatics* **30**, 523-530 (2014).

29. Zhang, X. *et al.* Depletion of BATF in CAR-T cells enhances antitumor activity by inducing resistance against exhaustion and formation of central memory cells. *Cancer Cell* **40**, 1407-1422.e1407 (2022).

30. Seo, H. *et al.* BATF and IRF4 cooperate to counter exhaustion in tumor-infiltrating CAR T cells. *Nat Immunol* **22**, 983-995 (2021).

31. Lynn, R.C. *et al.* c-Jun overexpression in CAR T cells induces exhaustion resistance. *Nature* **576**, 293-300 (2019).

32. van der Heide, V., Humblin, E., Vaidya, A. & Kamphorst, A.O. Advancing beyond the twists and turns of T cell exhaustion in cancer. *Sci Transl Med* **14**, eabo4997 (2022).

33. Chen, J. *et al.* NR4A transcription factors limit CAR T cell function in solid tumours. *Nature* **567**, 530-534 (2019).

34. Jung, I.Y. *et al.* BLIMP1 and NR4A3 transcription factors reciprocally regulate antitumor CAR T cell stemness and exhaustion. *Sci Transl Med* **14**, eabn7336 (2022).

35. Tandon, M. *et al.* Runx2 mediates epigenetic silencing of the bone morphogenetic protein-3B (BMP-3B/GDF10) in lung cancer cells. *Mol Cancer* **11**, 27 (2012).

36. Hojo, H. *et al.* Runx2 regulates chromatin accessibility to direct the osteoblast program at neonatal stages. *Cell Rep* **40**, 111315 (2022).

37. Wang, L. *et al.* TET enzymes regulate skeletal development through increasing chromatin accessibility of RUNX2 target genes. *Nat Commun* **13**, 4709 (2022).

38. Korinfskaya, S., Parameswaran, S., Weirauch, M.T. & Barski, A. Runx Transcription Factors in T Cells-What Is Beyond Thymic Development? *Front Immunol* **12**, 701924 (2021).

39. Kochenderfer, J.N., Yu, Z., Frasheri, D., Restifo, N.P. & Rosenberg, S.A. Adoptive transfer of syngeneic T cells transduced with a chimeric antigen receptor that recognizes murine CD19 can eradicate lymphoma and normal B cells. *Blood* **116**, 3875-3886 (2010).

METHODS REFERENCES

40. Corces, M.R. *et al.* An improved ATAC-seq protocol reduces background and enables interrogation of frozen tissues. *Nat Methods* **14**, 959-962 (2017).

41. Buenrostro, J.D. *et al.* Single-cell chromatin accessibility reveals principles of regulatory variation. *Nature* **523**, 486-490 (2015).

42. Wingett, S.W. & Andrews, S. FastQ Screen: A tool for multi-genome mapping and quality control. *F1000Res* **7**, 1338 (2018).

43. Ewels, P., Magnusson, M., Lundin, S. & Käller, M. MultiQC: summarize analysis results for multiple tools and samples in a single report. *Bioinformatics* **32**, 3047-3048 (2016).

44. Dobin, A. *et al.* STAR: ultrafast universal RNA-seq aligner. *Bioinformatics* **29**, 15-21 (2013).

45. Love, M.I., Huber, W. & Anders, S. Moderated estimation of fold change and dispersion for RNA-seq data with DESeq2. *Genome Biol* **15**, 550 (2014).

46. Zhu, A., Srivastava, A., Ibrahim, J.G., Patro, R. & Love, M.I. Nonparametric expression analysis using inferential replicate counts. *Nucleic Acids Res* **47**, e105 (2019).

47. Zhou, Y. *et al.* Metascape provides a biologist-oriented resource for the analysis of systems-level datasets. *Nat Commun* **10**, 1523 (2019).

48. Mootha, V.K. *et al.* PGC-1alpha-responsive genes involved in oxidative phosphorylation are coordinately downregulated in human diabetes. *Nat Genet* **34**, 267-273 (2003).

49. Quinlan, A.R. & Hall, I.M. BEDTools: a flexible suite of utilities for comparing genomic features. *Bioinformatics* **26**, 841-842 (2010).

50. Ritchie, M.E. *et al.* limma powers differential expression analyses for RNA-sequencing and microarray studies. *Nucleic Acids Res* **43**, e47 (2015).

51. Ramírez, F., Dündar, F., Diehl, S., Grüning, B.A. & Manke, T. deepTools: a flexible platform for exploring deep-sequencing data. *Nucleic Acids Res* **42**, W187-191 (2014).

1 FIGURES

Figure 1

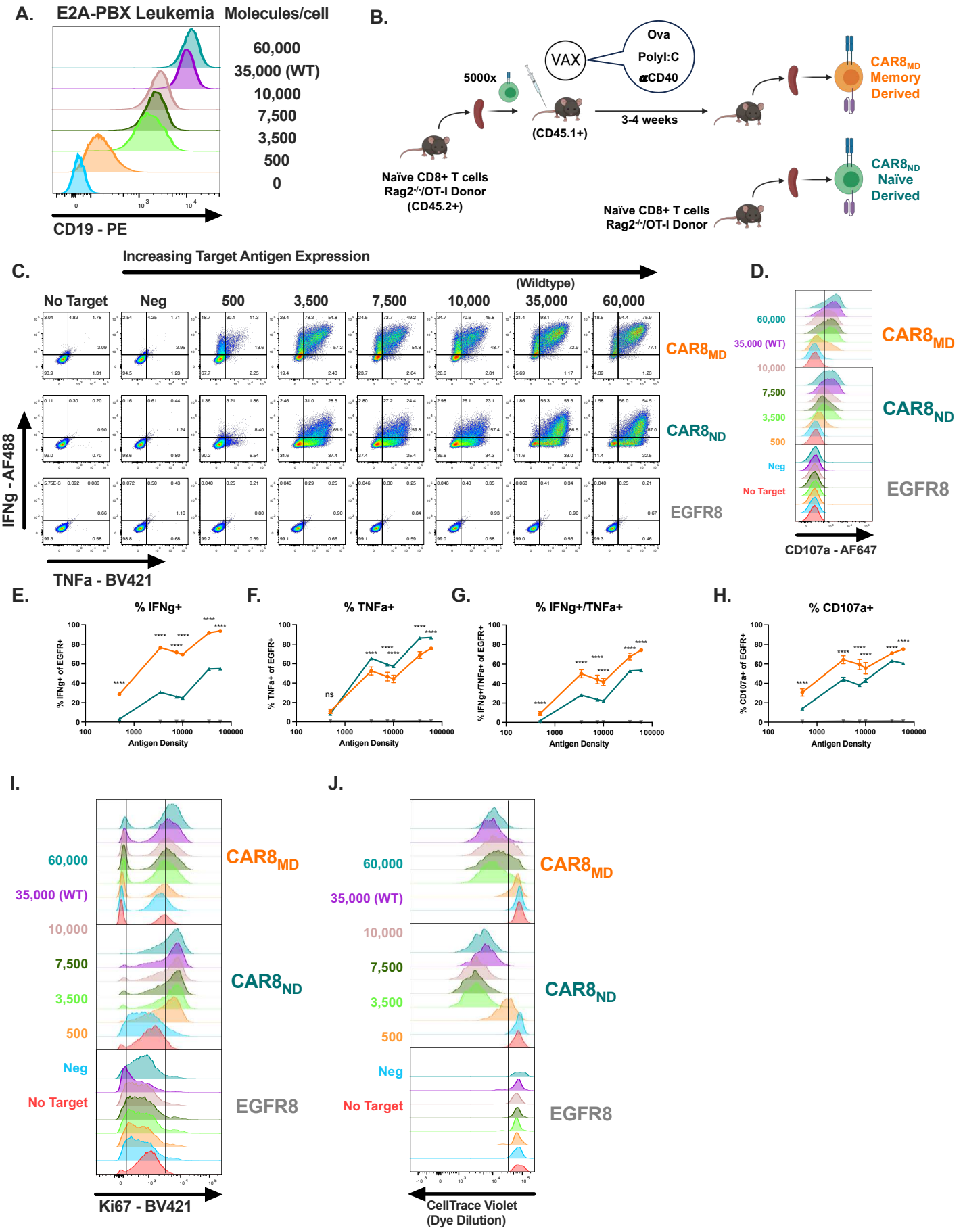

Figure 1: Antigen experience history directs multiple aspects of *in vitro* functional capacity of murine CD8+ CAR T cells.

1A: E2A-PBX murine leukemia was engineered to knockout CD19, followed by reintroduction of CD19 at different levels to generate a range of antigen density clones. **1B:** Schematic: Vaccine model for generating memory CD8+ OT-I T cells. 5e3 OT-I T cells were transferred into congenically distinct hosts which were concurrently vaccinated with antigen and adjuvants. 3-5 weeks later, CAR T cells were manufactured from memory OT-I's ($CAR8_{MD,}$ memory-derived) or naïve OT-I's ($CAR8_{ND}$, naïve-derived) **1C:** Intracellular cytokine staining of IFNg and TNFa after 6 hour co-culture assay. **1D:** Degranulation as measured by CD107a expression after 4 hour co-culture assay. **1E-G:** Quantification of cytokine data, % positive cells for indicated cytokine. **1H:** Quantification of CD107a data, % positive cells. **1I:** Cell-cycle entry as measured by Ki-67 staining after 18 hour co-culture assay. **1J:** Proliferation as measured by dilution of CellTrace Violet dye after 72 hour co-culture assay. All *in vitro* assays were performed with n=3 technical replicates, and are representative of 2 independent experiments. Data represent mean +/- SD. * $p<0.05$, ** $p<0.01$, *** $p<0.001$, **** $p<0.0001$.

Figure 2

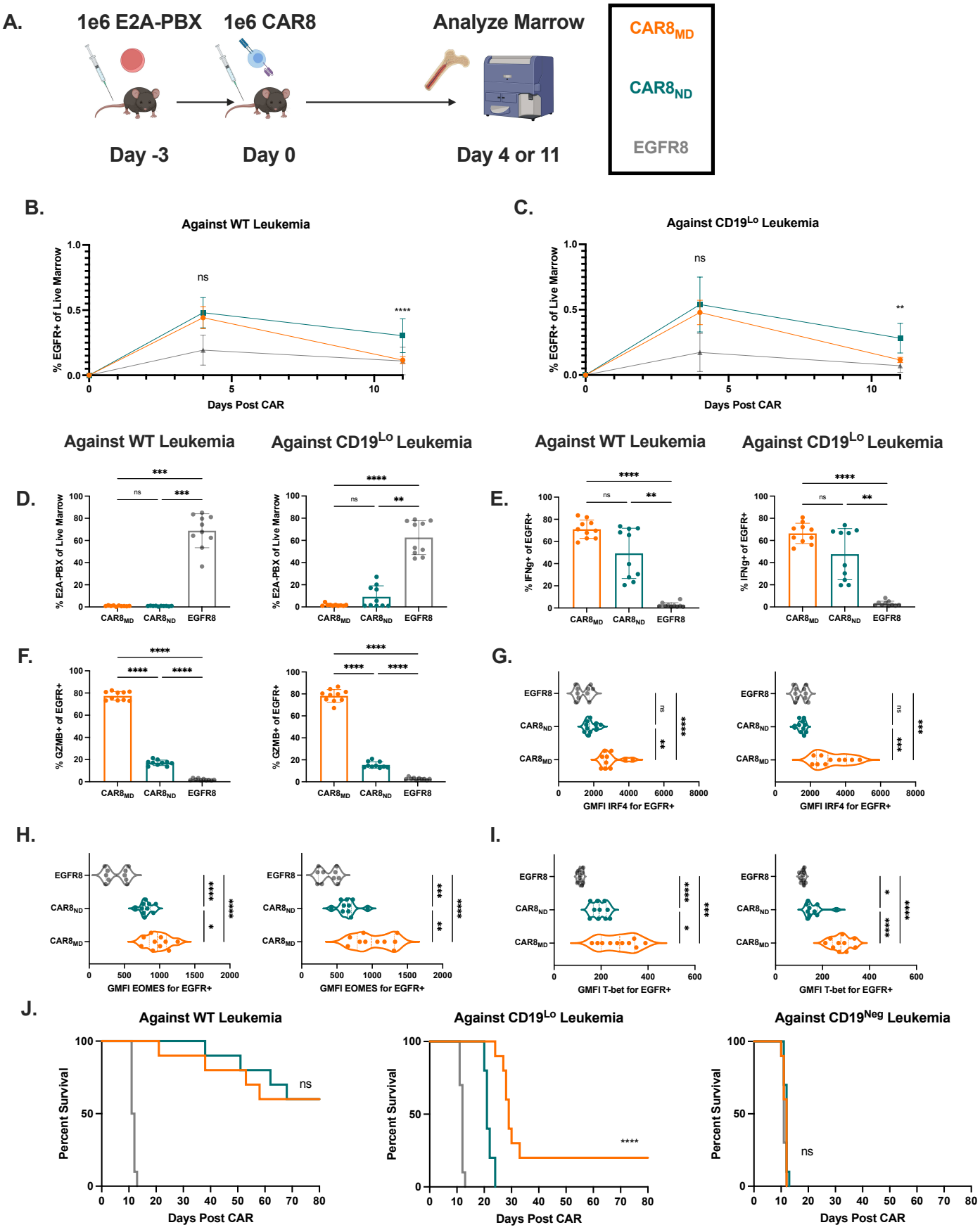
A.
1e6 E2A-PBX
1e6 CAR8
Analyze Marrow
Day -3
Day 0
Day 4 or 11
CAR8MD
CAR8ND
EGFR8
B.
Against WT Leukemia
% EGFR+ of Live Marrow
Days Post CAR
ns
****
C.
Against CD19Lo Leukemia
% EGFR+ of Live Marrow
Days Post CAR
ns
**
Against WT Leukemia
Against CD19Lo Leukemia
Against WT Leukemia
Against CD19Lo Leukemia
D.
% E2A-PBX of Live Marrow
E.
% IFNg+ of EGFR+
F.
% GZMB+ of EGFR+
G.
GMFI IRF4 for EGFR+
H.
GMFI EOMES for EGFR+
I.
GMFI T-bet for EGFR+
J.
Against WT Leukemia
Against CD19Lo Leukemia
Against CD19Neg Leukemia
Percent Survival
Days Post CAR
ns
****
ns

Figure 2: $CAR8_{MD}$ exhibit enhanced cytotoxicity and clearance of $CD19^{Lo}$ leukemia *in vivo* (high CAR dose).

2A: Schematic: Timeline for *in vivo* experiments. *Rag1*$^{-/-}$ mice were injected with 1e6 E2A-PBX1 leukemia on day -3, followed by 1e6 OT-I CD8+/EGFR+ T cells from indicated T cell condition on day 0. Bone marrow was analyzed by flow cytometry on day +4 or day +11. T cell populations were isolated memory-derived CAR T cells ($CAR8_{MD}$), isolated naïve-derived CAR T cells ($CAR8_{ND}$) or EGFR control T cells (EGFR8). Leukemia populations were $CD19^{Neg}$, $CD19^{Lo}$(10,000 antigens/cell), or WT (35,000 antigens/cell). **2B-C:** Early T cell expansion (day +4) or persistence (day +11) after infusion of transduced T cells against WT leukemia **(B)** and $CD19^{Lo}$ leukemia **(C)**. Transduced T cell populations measured by coexpression of CD8a+/TCRbeta+/EGFR+. **2D:** Clearance of WT and $CD19^{Lo}$ leukemia at day +11 after CAR infusion. E2A-PBX measured by coexpression of B220+/CD22+. **2E-F:** Intracellular cytokine staining of interferon gamma **(E)** or granzyme B **(F)** in CAR T cells from whole bone marrow restimulated *ex vivo* with leukemia. Data represent mean +/- SD. **2G-I:** Intranuclear transcription factor staining of IRF4 **(G)**, EOMES **(H)**, or T-bet **(I)** on CAR+ T cells from mice bearing the indicated leukemia at day +4 after CAR infusion. Violin plot data represent median with quartiles. Data are from 2 pooled, independent experiments with n=10 mice per condition. * $p<0.05$, ** $p<0.01$, *** $p<0.001$, **** $p<0.0001$. **2J:** Survival of mice after treatment with 1e6 EGFR+ CAR or control T cells. Survival statistics were performed using log-rank (Mantel-Cox) test * $p<0.05$, ** $p<0.01$, *** $p<0.001$, **** $p<0.0001$. Data is from 2 independent pooled experiments, total n=10 mice per group.

Figure 3

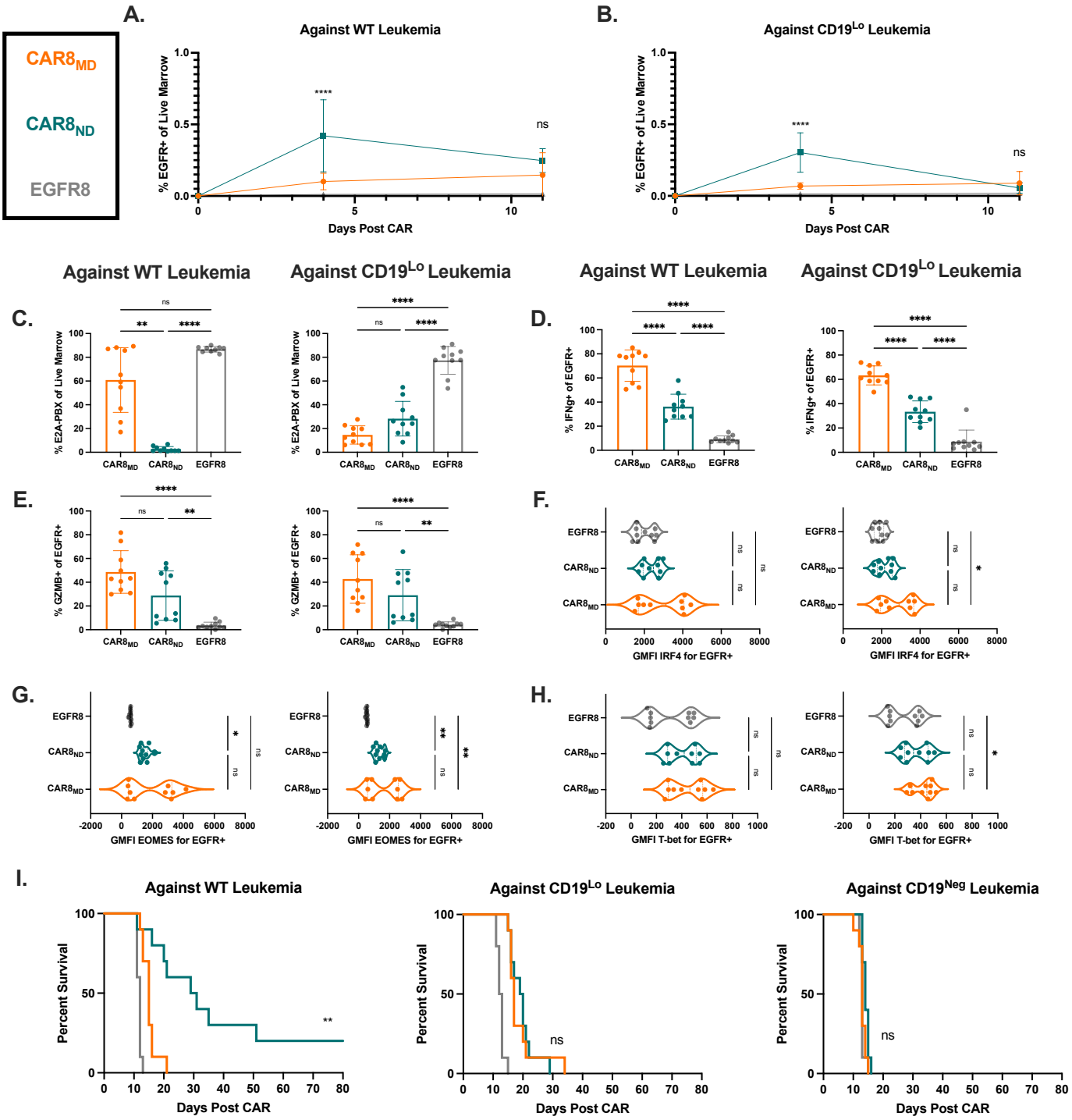
A.
Against WT Leukemia
CAR8MD
CAR8ND
EGFR8
% EGFR+ of Live Marrow
Days Post CAR
****
ns
B.
Against CD19Lo Leukemia
C.
Against WT Leukemia
Against CD19Lo Leukemia
% E2A-PBX of Live Marrow
D.
Against WT Leukemia
Against CD19Lo Leukemia
% IFNg+ of EGFR+
E.
% GZMB+ of EGFR+
F.
GMFI IRF4 for EGFR+
G.
GMFI EOMES for EGFR+
H.
GMFI T-bet for EGFR+
I.
Against WT Leukemia
Against CD19Lo Leukemia
Against CD19Neg Leukemia
Percent Survival
Days Post CAR

Figure 3: $CAR8_{ND}$ exhibit enhanced expansion capacity and clearance of WT leukemia *in vivo* (low CAR dose).

3A-B: Early T cell expansion (day +4) or persistence (day +11) after infusion of transduced T cells against WT leukemia **(A)** and $CD19^{Lo}$ leukemia **(B)**. Transduced T cell populations measured by coexpression of CD8a+/TCRbeta+/EGFR+. **3C:** Clearance of WT and $CD19^{Lo}$ leukemia at day +11 after CAR infusion. E2A-PBX measured by coexpression of B220+/CD22+. **3D-E:** Intracellular cytokine staining of interferon gamma **(D)** or granzyme B **(E)** in CAR T cells from whole bone marrow restimulated *ex vivo* with leukemia. Data represent mean +/- SD. **2F-H:** Intranuclear transcription factor staining of IRF4 **(F)**, EOMES **(G)**, or T-bet **(H)** on CAR+ T cells from mice bearing the indicated leukemia at day +4 after CAR infusion. Violin plot data represent median with quartiles. Data are from 2 pooled, independent experiments with n=10 mice per condition. * $p<0.05$, ** $p<0.01$, *** $p<0.001$, **** $p<0.0001$. **2I:** Survival of mice after treatment with 1e6 EGFR+ CAR or control T cells. * $p<0.05$, ** $p<0.01$, *** $p<0.001$, **** $p<0.0001$. Data are from 2 independent pooled experiments, total n=10 mice per group.

Figure 4

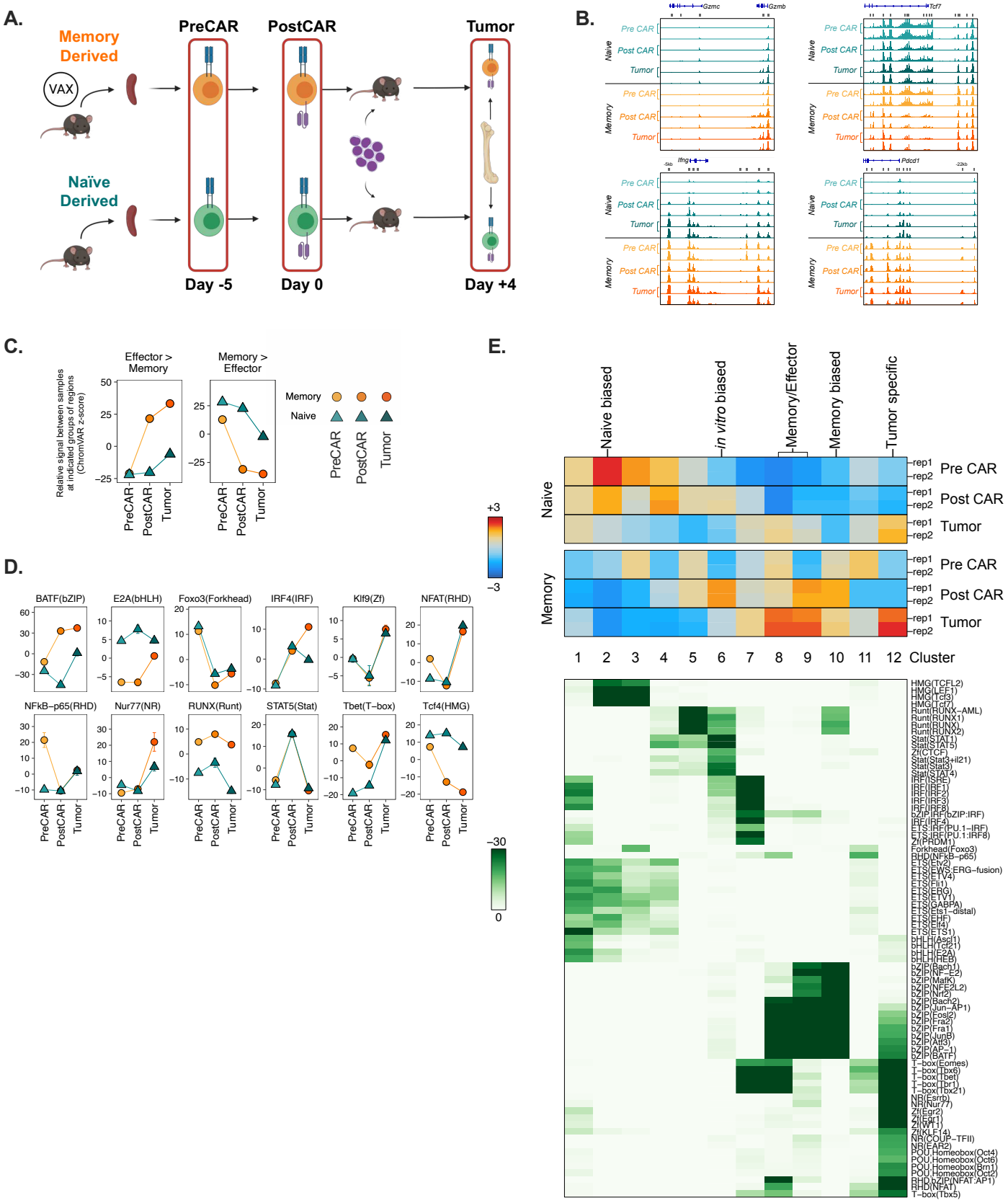
A.
Memory Derived
Naïve Derived
VAX
PreCAR
PostCAR
Tumor
Day -5
Day 0
Day +4
B.
Gzmc
Gzmb
Tcf7
Ifng
Pdcd1
Pre CAR
Post CAR
Tumor
Naive
Memory
C.
Effector > Memory
Memory > Effector
Relative signal between samples at indicated groups of regions (ChromVAR z-score)
Memory
Naive
PreCAR
PostCAR
Tumor
D.
BATF(bZIP)
E2A(bHLH)
Foxo3(Forkhead)
IRF4(IRF)
Klf9(Zf)
NFAT(RHD)
NFkB–p65(RHD)
Nur77(NR)
RUNX(Runt)
STAT5(Stat)
Tbet(T–box)
Tcf4(HMG)
+3
–3
–30
0
E.
Naive biased
in vitro biased
Memory/Effector
Memory biased
Tumor specific
Naive
Memory
rep1
rep2
Pre CAR
Post CAR
Tumor
1 2 3 4 5 6 7 8 9 10 11 12 Cluster
HMG(TCFL2)
HMG(LEF1)
HMG(Tcf3)
HMG(Tcf7)
Runt(RUNX–AML)
Runt(RUNX1)
Runt(RUNX)
Runt(RUNX2)
Stat(STAT1)
Stat(STAT5)
Zf(CTCF)
Stat(Stat3+il21)
Stat(Stat3)
Stat(STAT4)
IRF(ISRE)
IRF(IRF1)
IRF(IRF2)
IRF(IRF3)
IRF(IRF8)
bZIP:IRF(bZIP:IRF)
IRF(IRF4)
ETS:IRF(PU.1–IRF)
ETS:IRF(PU.1:IRF8)
Zf(PRDM1)
Forkhead(Foxo3)
RHD(NFkB–p65)
ETS(Etv2)
ETS(EWS:ERG–fusion)
ETS(ETV4)
ETS(Fli1)
ETS(ERG)
ETS(ETV1)
ETS(GABPA)
ETS(Ets1–distal)
ETS(EHF)
ETS(Elf4)
ETS(ETS1)
bHLH(Ascl1)
bHLH(Tcf21)
bHLH(E2A)
bHLH(HEB)
bZIP(Bach1)
bZIP(NF–E2)
bZIP(MafK)
bZIP(NFE2L2)
bZIP(Nrf2)
bZIP(Bach2)
bZIP(Jun–AP1)
bZIP(Fosl2)
bZIP(Fra2)
bZIP(Fra1)
bZIP(JunB)
bZIP(Atf3)
bZIP(BAP–1)
bZIP(BATF)
T–box(Eomes)
T–box(Tbx6)
T–box(Tbet)
T–box(Tbr1)
T–box(Tbx21)
NR(Esrrb)
NR(Nur77)
Zf(Egr2)
Zf(Egr1)
Zf(WT1)
Zf(KLF14)
NR(COUP–TFII)
NR(EAR2)
POU:Homeobox(Oct4)
POU:Homeobox(Oct6)
POU:Homeobox(Brn1)
POU:Homeobox(Oct2)
RHD:bZIP(NFAT:AP1)
RHD(NFAT)
T–box(Tbx5)

Figure 4: Prior antigen experience imprints chromatin accessibility states which follow unique patterns during CAR transduction and reinfusion.

4A: Schematic: Layout for paired ATAC-seq/RNA-seq experiments. Memory-derived or naïve derived OT-I CD8+ T cells were sorted at three sequential timepoints: *Ex vivo* from donor mice before CAR transduction ("PreCAR"), *in vitro* after CAR transduction ("PostCAR"), and *ex vivo* after reinfusion into $CD19^{Lo}$ leukemia-bearing *Rag1*$^{-/-}$ mice ("Tumor"). **4B:** Chromatin accessibility at *Gzmb, Gzmc, Ifng, Tcf7 and Pdcd1* gene loci for naïve and memory-derived T cells at each timepoint. **4C:** ChromVAR deviation z-scores between indicated populations at differentially accessible regions between Effector and Memory T cells after LCMV-Armstrong infection[23]. Data are mean +/- range of two biological replicates. **4D:** Motif-associated ChromVAR deviation z-scores between indicated populations. Data are mean +/- range of two biological replicates **4E:** K-means clustering of relative ATAC-seq signal at differentially accessible regions (top, data from two biological replicates are shown) and motif enrichment in each cluster vs all regions (bottom).

Figure 5

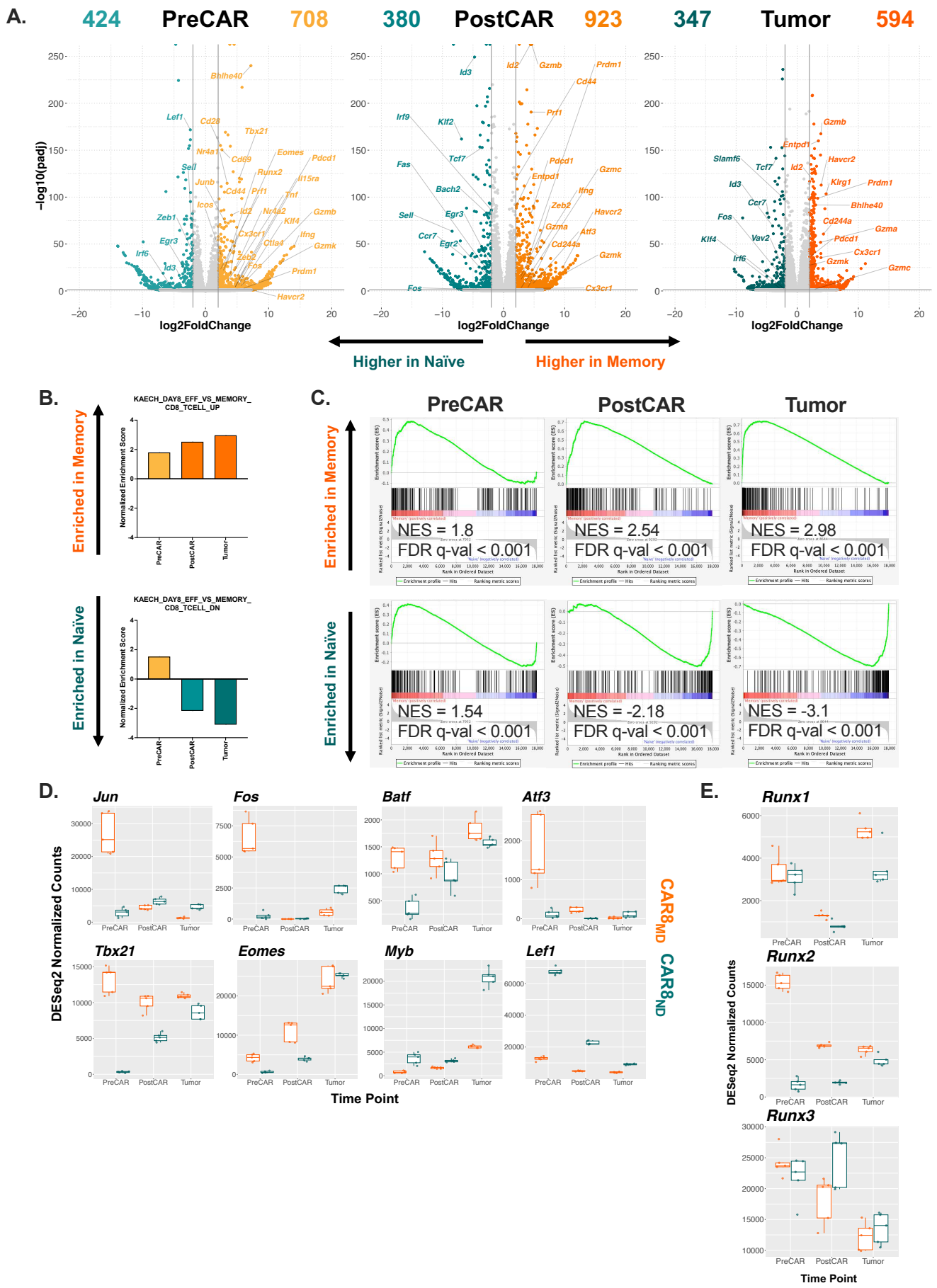
A.
424
PreCAR
708
380
PostCAR
923
347
Tumor
594
−log10(padj)
log2FoldChange
Higher in Naïve
Higher in Memory
B.
Enriched in Memory
KAECH_DAY8_EFF_VS_MEMORY_CD8_TCELL_UP
Normalized Enrichment Score
PreCAR
PostCAR
Tumor
Enriched in Naïve
KAECH_DAY8_EFF_VS_MEMORY_CD8_TCELL_DN
C.
PreCAR
PostCAR
Tumor
Enriched in Memory
NES = 1.8
FDR q-val < 0.001
NES = 2.54
FDR q-val < 0.001
NES = 2.98
FDR q-val < 0.001
Enriched in Naïve
NES = 1.54
FDR q-val < 0.001
NES = -2.18
FDR q-val < 0.001
NES = -3.1
FDR q-val < 0.001
D.
Jun
Fos
Batf
Atf3
Tbx21
Eomes
Myb
Lef1
DESeq2 Normalized Counts
Time Point
CAR8MD
CAR8ND
E.
Runx1
Runx2
Runx3
DESeq2 Normalized Counts
Time Point

Figure 5: Prior antigen experience drives differential CAR8 transcriptomic states which follow unique patterns during CAR transduction and reinfusion.

RNA-seq analysis was run on the timepoints/conditions indicated in the previous figure. **5A:** Volcano plots of significant differentially expressed genes between naïve and memory-derived cells at each of the three timepoints. **5B:** Normalized enrichment scores from gene set enrichment analysis (GSEA) of differentially enriched genesets between indicated CD8+ T cell subsets after LCMV-Armstrong acute viral infection[24] **5C:** GSEA plots at each timepoint. **5D:** Top differentially expressed transcription factors at the “PreCAR” timepoint, generated using Ingenuity Pathway Analysis (IPA). **5E:** DESeq2-normalized counts of indicated transcription factors at each timepoint for naïve and memory-derived cells. **5F:** DESeq2-normalized counts of Runx family transcription factors at each timepoint for naïve and memory-derived cells. All statistics performed using DESeq2 with filtering threshold at 10, log2foldchange >2 and padj < 0.05.

Figure 6

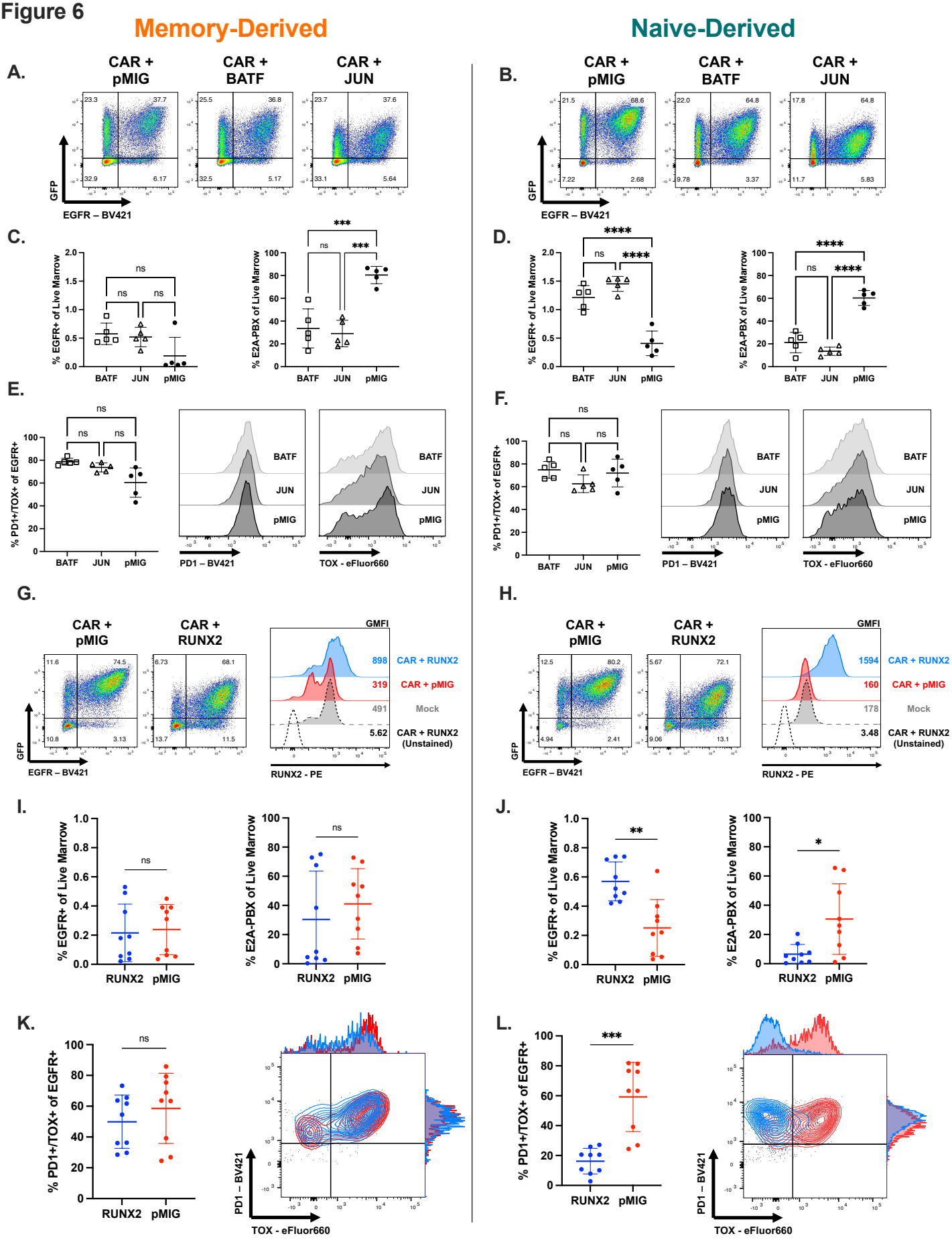
Memory-Derived
Naive-Derived
A.
B.
CAR + pMIG
CAR + BATF
CAR + JUN
GFP
EGFR – BV421
C.
D.
% EGFR+ of Live Marrow
% E2A-PBX of Live Marrow
BATF
JUN
pMIG
ns
***
****
E.
F.
% PD1+/TOX+ of EGFR+
PD1 – BV421
TOX - eFluor660
G.
H.
CAR + RUNX2
GMFI
898
319
491
5.62
CAR + RUNX2
CAR + pMIG
Mock
CAR + RUNX2 (Unstained)
RUNX2 - PE
1594
160
178
3.48
I.
J.
RUNX2
pMIG
**
*
K.
L.

Figure 6: Runx2 overexpression as a novel strategy for enhancement of naïve-derived CD8+ CAR T cell potency and resistance to dysfunction.

6A-B: Cotransduction of memory (A) or naïve (B) CD8+ T cells with CAR and pMIG-Empty, pMIG-BATF, or pMIG-JUN**.** For **6C-F & I-L**, *Rag1*$^{-/-}$ mice were given leukemia on day -3, followed by 1e5 pMIG-Runx2 or pMIG-Empty co-transduced CAR8 on day 0. Bone marrow was analyzed by flow cytometry on day 11 post-CAR. **6C & D:** CAR T cell and leukemia proportions for naïve (C) and memory-derived (D) CAR T cells cotransduced with BATF, JUN or pMIG control. **6E & F:** Proportion of CAR T cells displaying PD1+/TOX+ phenotype. **6G-H:** Cotransduction of memory (G) or naïve (H) CD8+ T cells with CAR and pMIG-Empty or pMIG-Runx2 **and** intracellular staining for Runx2. **6I & J:** CAR T cell and leukemia proportions for naïve (C) and memory-derived (D) CAR T cells cotransduced with RUNX2 or pMIG control. **6K & L:** Proportion of CAR T cells displaying PD1+/TOX+ phenotype. Data in 6A,B,G & H are representative of 3-4 independent experiments. Data in 6C-F are from 1 experiment with n=5 mice per condition. Data in 6I-L are from 2 pooled, independent experiments with n=9 mice per condition. Data represent mean +/- SD. * $p<0.05$, ** $p<0.01$, *** $p<0.001$, **** $p<0.0001$.

Figure S1

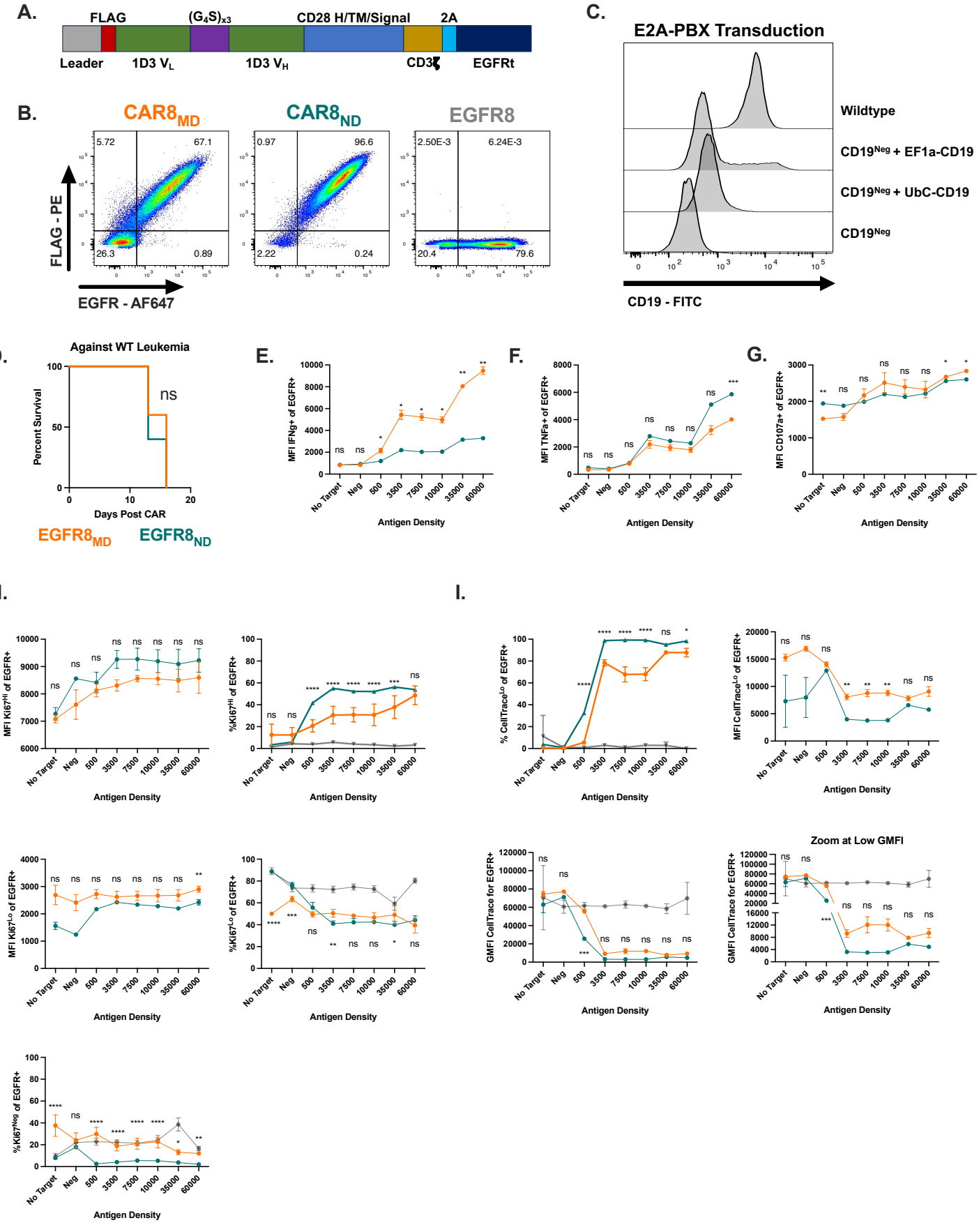
A.
FLAG
(G4S)x3
CD28 H/TM/Signal
2A
Leader
1D3 VL
1D3 VH
CD3ζ
EGFRt
B.
CAR8MD
CAR8ND
EGFR8
5.72
67.1
26.3
0.89
0.97
96.6
2.22
0.24
2.50E-3
6.24E-3
20.4
79.6
FLAG - PE
EGFR - AF647
C.
E2A-PBX Transduction
Wildtype
CD19Neg + EF1a-CD19
CD19Neg + UbC-CD19
CD19Neg
CD19 - FITC
D.
Against WT Leukemia
Percent Survival
Days Post CAR
ns
EGFR8MD
EGFR8ND
E.
MFI IFNg+ of EGFR+
F.
MFI TNFa+ of EGFR+
G.
MFI CD107a+ of EGFR+
No Target
Neg
500
3500
7500
10000
35000
60000
Antigen Density
H.
MFI KI67Hi of EGFR+
%KI67Hi of EGFR+
MFI KI67Lo of EGFR+
%KI67Lo of EGFR+
%KI67Neg of EGFR+
I.
% CellTraceLo of EGFR+
MFI CellTraceLo of EGFR+
GMFI CellTrace for EGFR+
Zoom at Low GMFI

Figure S1: E2A-PBX/mCD19 antigen density model and murine anti-CD19 CAR T cells, and additional statistical comparisons of *in vitro* data (Related to Figure 1)

S1A: Schematic of the anti-mouse CD19 CAR contained in pMSCV backbone. **S1B:** Coexpression of CAR and EGFR on murine CAR T cells. **S1C:** Engineering of murine leukemia with lentiviral vectors containing hUbC or hEF1a promoters driving the CD19 transgene. **S1D:** Survival of mice after treatment with 1e6 EGFR+ (EGFR8, non-CAR expressing) naïve or memory-derived CD8+ T cells. Data is from 1 experiment, total n=5 mice per group. **S1E:** Mean fluorescence intensity of IFNg+ cell population. **S1F:** Mean fluorescence intensity of TNFa+ cell population. **S1G:** Mean fluorescence intensity of CD107a+ population. **S1H:** Statistical comparisons of $Ki67^{Neg}$ (% Ki67Neg of EGFR+), $Ki67^{Lo}$(%$Ki67^{Lo}$ of EGFR+, MFI $Ki67^{Lo}$ of EGFR+) and $Ki67^{Hi}$(%$Ki67^{Hi}$ of EGFR+, MFI $Ki67^{Hi}$ of EGFR+) populations . **S1I:** Statistical comparisons of $CellTrace^{Lo}$ (% $CellTrace^{Lo}$ of EGFR+, MFI $CellTrace^{Lo}$ of EGFR+) and total EGFR+ (GFMI CellTrace, GFMI CellTrace with zoomed axis) populations. Data represent mean +/- SD. * $p<0.05$, ** $p<0.01$, *** $p<0.001$, **** $p<0.0001$.

Figure S2

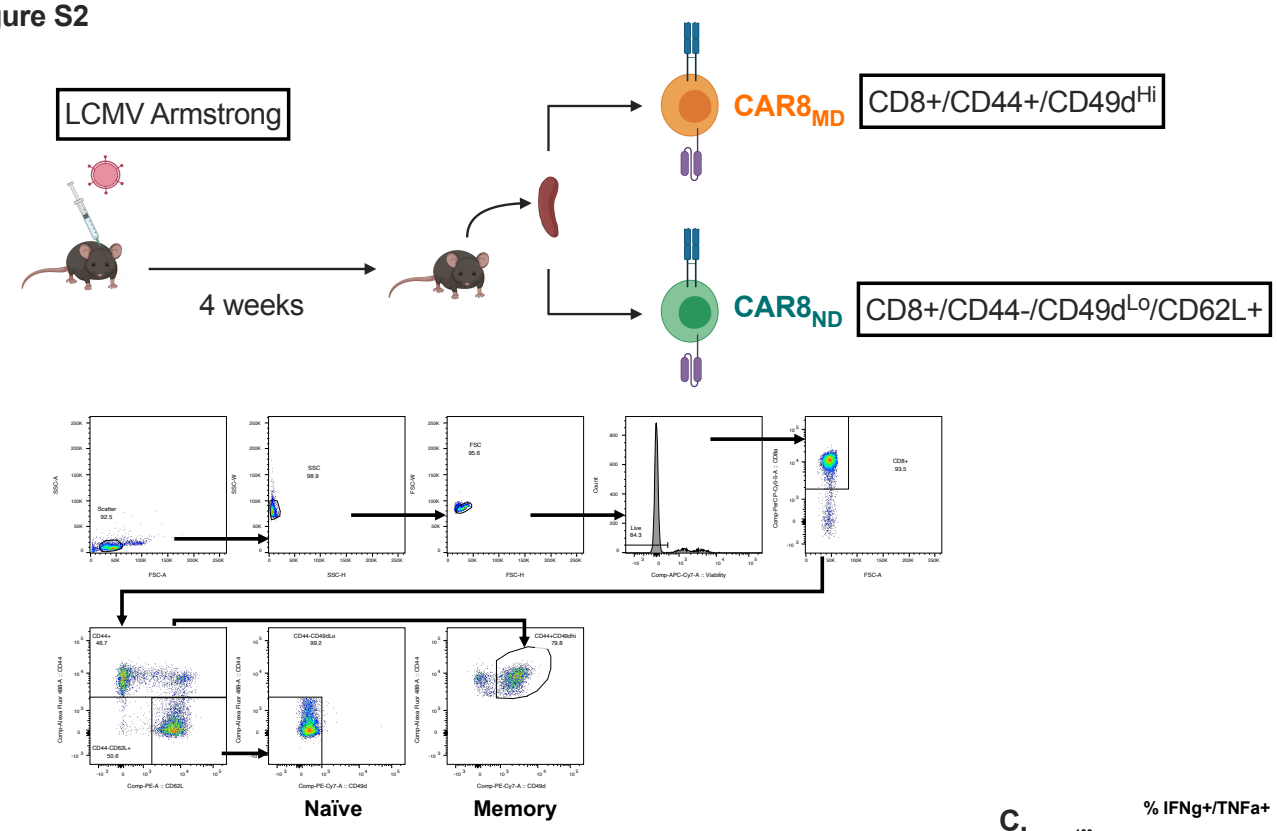
A.
LCMV Armstrong
4 weeks
CAR8MD
CD8+/CD44+/CD49dHi
CAR8ND
CD8+/CD44-/CD49dLo/CD62L+
Naïve
Memory

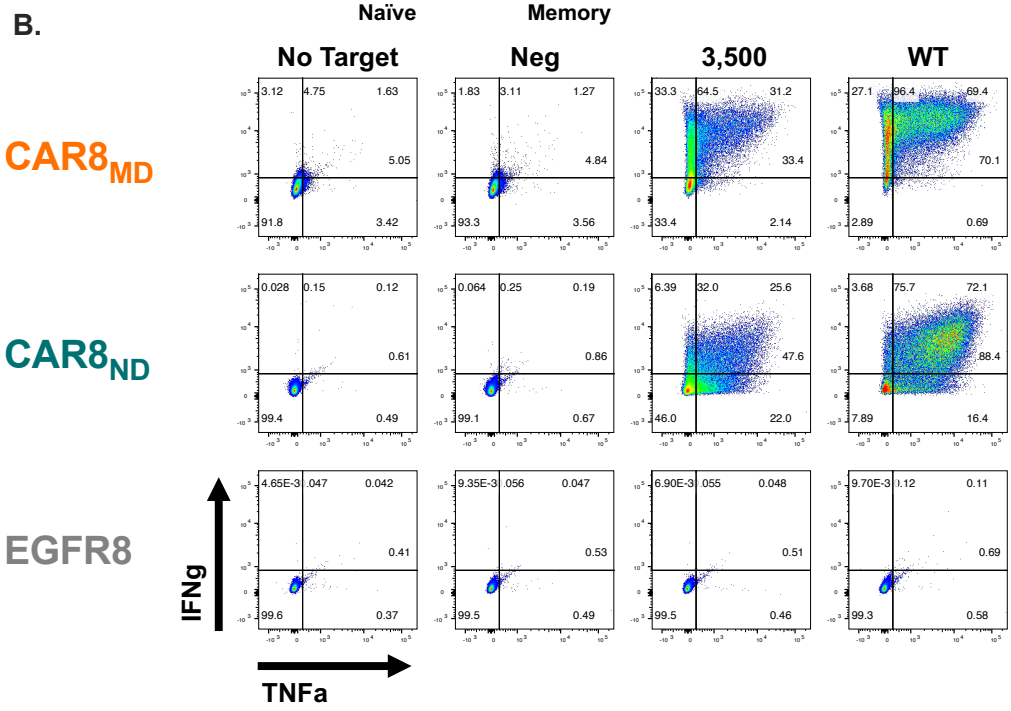
B.
No Target
Neg
3,500
WT
CAR8MD
CAR8ND
EGFR8
IFNg
TNFa

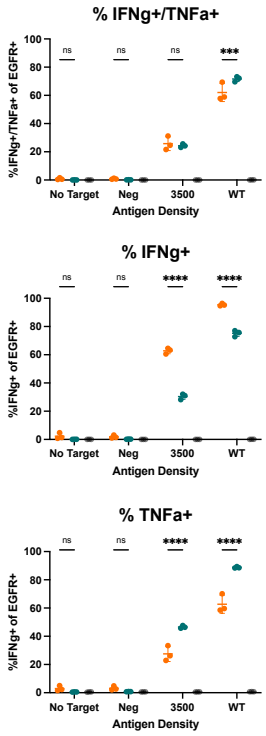
C.
% IFNg+/TNFa+
% IFNg+
% TNFa+
%IFNg+/TNFa+ of EGFR+
%IFNg+ of EGFR+
No Target
Neg
3500
WT
Antigen Density

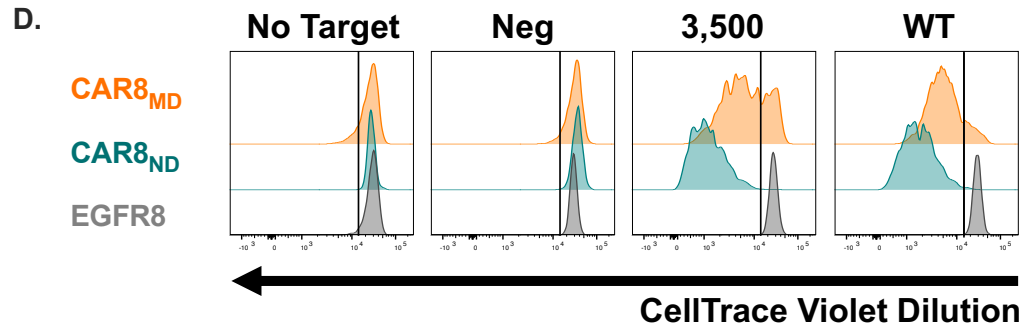
D.
No Target
Neg
3,500
WT
CAR8MD
CAR8ND
EGFR8
CellTrace Violet Dilution

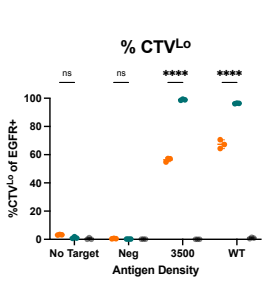
E.
% CTVLo
%CTVLo of EGFR+
No Target
Neg
3500
WT
Antigen Density

Figure S2: Polyclonal pathogen-elicited $CAR8_{MD}$ function similarly to vaccine-elicited $CAR8_{MD}$ (Related to Figure 1).

S3A: Schematic: LCMV model for generating memory CD8+ T cells. C57BL/6 hosts were infected with LCMV-Armstrong. 4 weeks later, naïve and memory CD8+ T cells were sorted from the same hosts using the indicated FACS markers and used to manufacture $CAR8_{MD,}$ memory-derived or $CAR8_{ND}$, naïve-derived or EGFR8 control cells. **S3B:** Intracellular cytokine staining of IFNg and TNFa after 6 hour co-culture assay. **S3C:** Quantifications of proportions of IFNg+ and TNFa+ cells of EGFR+ population. **S3D:** Proliferation as measured by dilution of CellTrace Violet dye after 72 hour co-culture assay. **S3E:** Quantification of CellTrace assay, proportions of $CellTrace^{Lo}$ cells. All assays were performed with n=3 technical replicates, and are representative of 2 independent experiments. Data represent mean +/- SD. * $p<0.05$, ** $p<0.01$, *** $p<0.001$, **** $p<0.0001$.

Figure S3

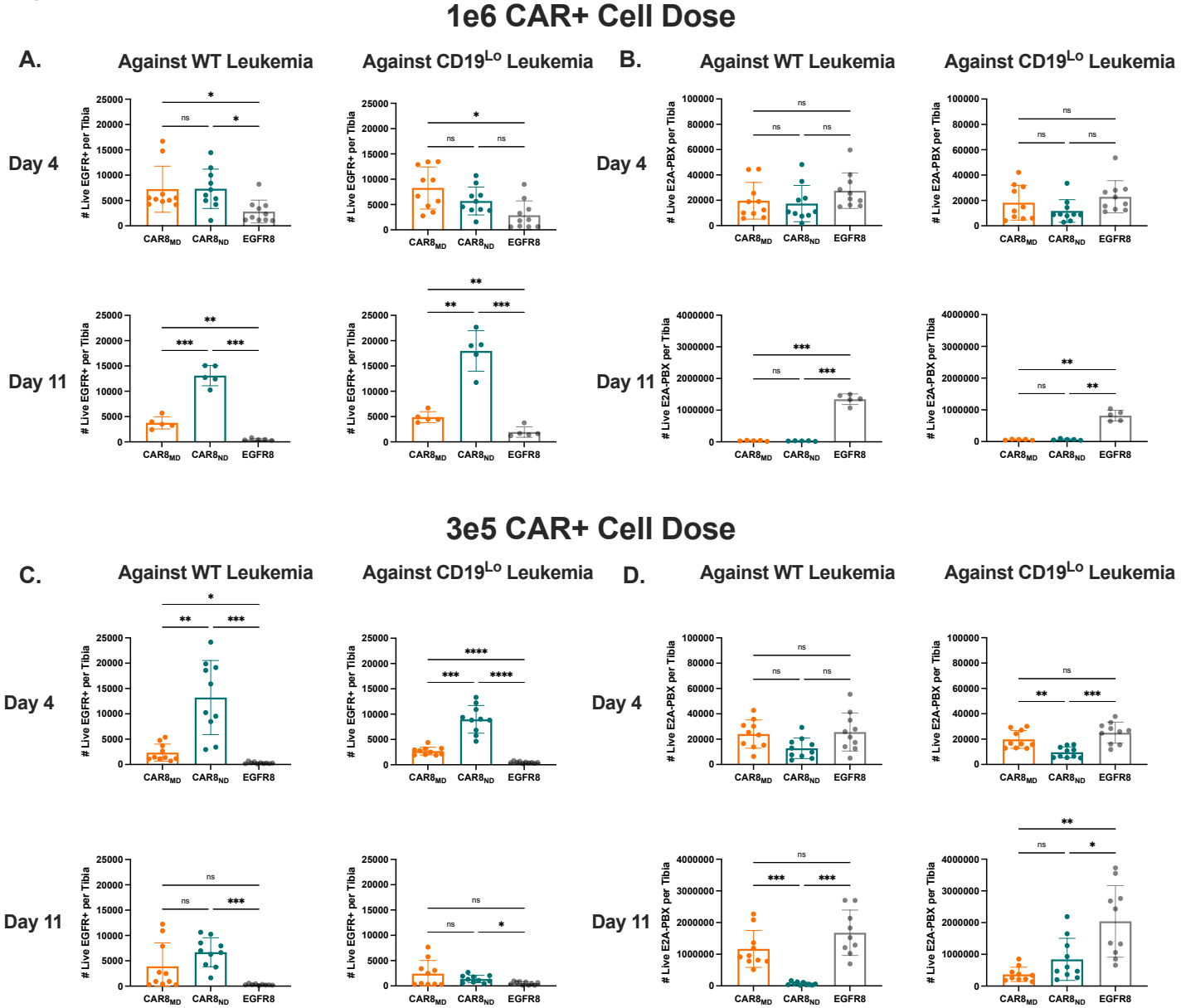

Figure S3: CAR T cells and leukemia counts per tibia for *in vivo* data (Related to Figures 2 & 3)

All analyses in this figure are done on the same experiments described in Figures 2 and 3. Counts data was generated by flushing a single tibia and using total tibia counts and cytometer proportions data to calculate CAR and leukemia cell counts per tibia. **S8A:** CAR counts for 1e6 CAR dose experiments. **S8B:** Leukemia counts for 1e6 CAR dose experiments. **S8C:** CAR counts for 3e5 CAR dose experiments. **S8D:** Leukemia counts for 3e5 CAR dose experiments. Data are from 2 pooled, independent experiments with n=10 mice per condition, apart from the 1e6 CAR dose day 11 timepoint, which contains data from one experiment with n=5 mice per condition. Data represent mean +/- SD. * p<0.05, ** p<0.01, *** p<0.001, **** p<0.0001.

Figure S4

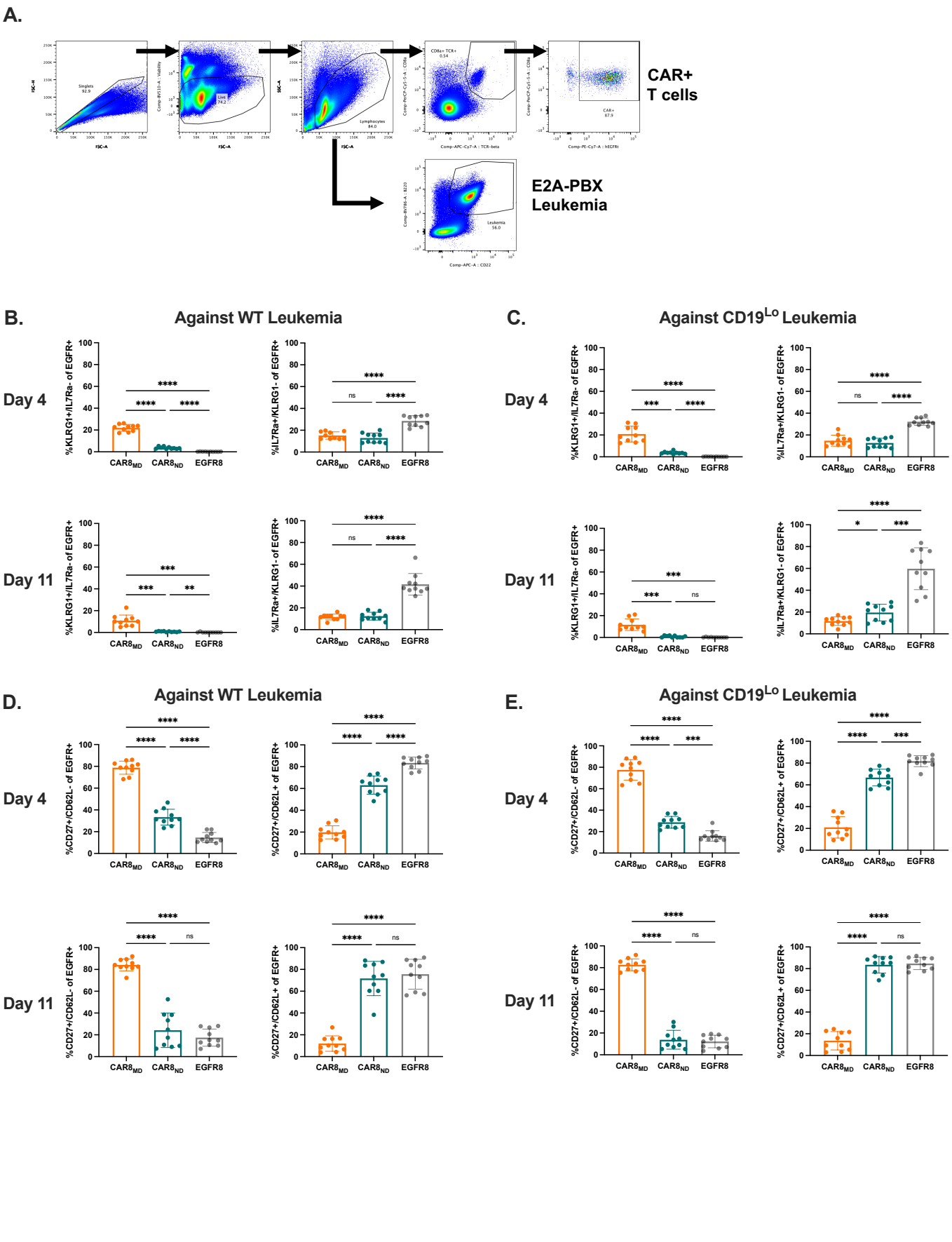
A.
CAR+
T cells
E2A-PBX
Leukemia
B.
Against WT Leukemia
C.
Against CD19Lo Leukemia
Day 4
Day 11
%KLRG1+/IL7Ra- of EGFR+
%IL7Ra+/KLRG1- of EGFR+
D.
Against WT Leukemia
E.
Against CD19Lo Leukemia
%CD27+/CD62L- of EGFR+
%CD27+/CD62L+ of EGFR+
CAR8MD
CAR8ND
EGFR8

Figure S4: Basic characterization of *in vivo* model and additional *in vivo* effector/memory phenotyping at high CAR dose (Related to Figure 2).

S4A: Basic flow cytometry gating strategy for *in vivo* experiments. Total events were gated by Singlets, Live Cells and then Lymphocytes, followed by CD8a+/TCRbeta+/EGFR+ cells for CAR8/EGFR8 or B220+/CD22+ cells for E2A-PBX. S4C-F are from experiments with the 1e6 EGFR+ cell dose. **S4B:** Proportions of CAR8 with the short-lived effector cell (SLEC, IL7Ra-/KLRG1+) or memory precursor effector cell (MPEC, IL7Ra+/KLRG1-) phenotypes at the indicated timepoint against WT leukemia. **S4C:** Proportions of CAR8 with the short-lived effector cell (SLEC, IL7Ra-/KLRG1+) or memory precursor effector cell (MPEC, IL7Ra+/KLRG1-) phenotypes at the indicated timepoint against $CD19^{Lo}$ leukemia. **S4D:** Proportions of CAR8 with the effector memory precursor (EMP, CD27+/CD62L-) or central memory precursor (CMP, CD27+/CD62L+) phenotypes at the indicated timepoint against WT leukemia. **S4E:** Proportions of CAR8 with the effector memory precursor (EMP, CD27+/CD62L-) or central memory precursor (CMP, CD27+/CD62L+) phenotypes at the indicated timepoint against $CD19^{Lo}$ leukemia. Data in S4C-F are from 2 pooled, independent experiments with n=10 mice per condition. Data represent mean +/- SD. * $p<0.05$, ** $p<0.01$, *** $p<0.001$, **** $p<0.0001$.

Figure S5

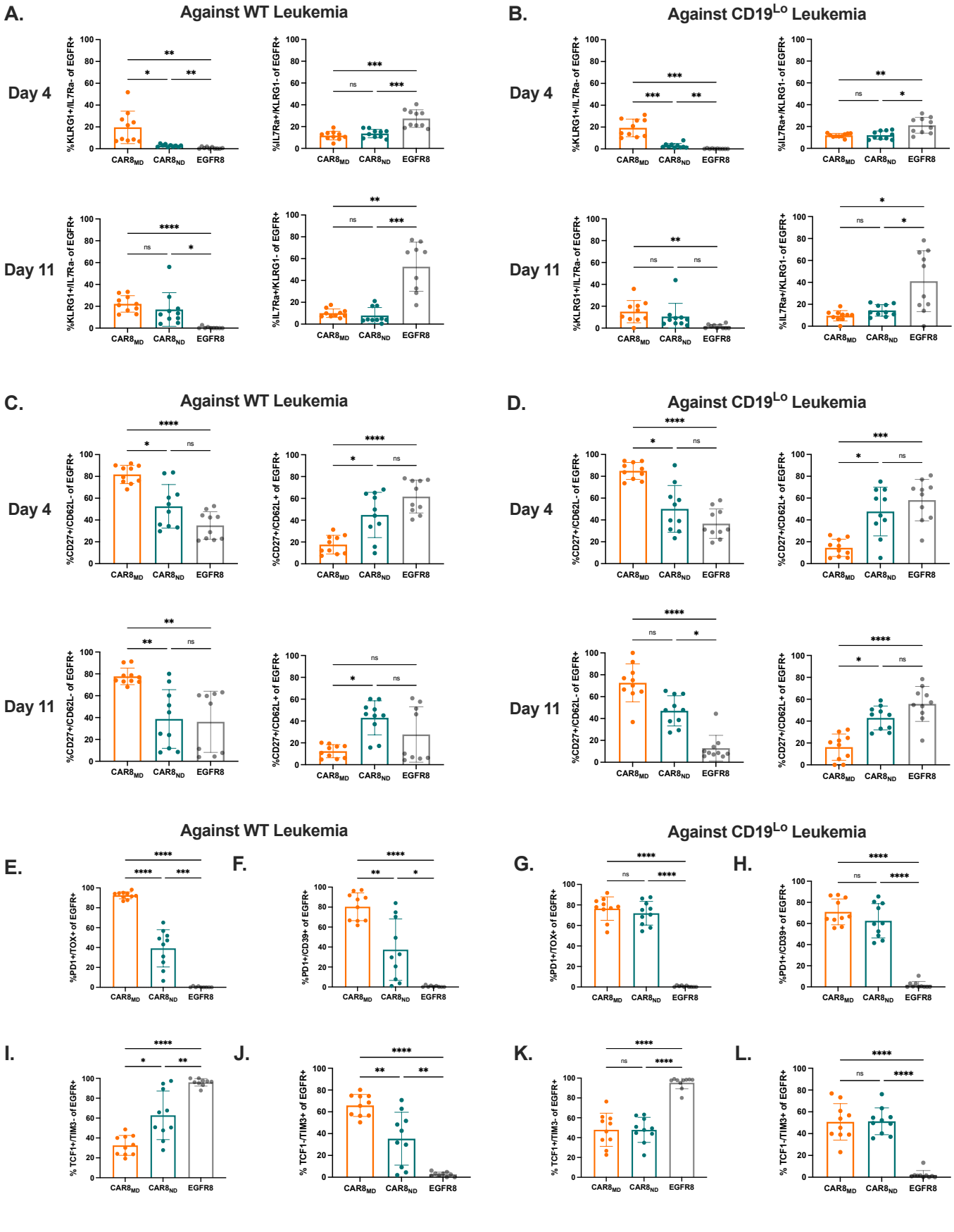
A.
Against WT Leukemia
Day 4
Day 11
%KLRG1+/IL7Ra- of EGFR+
%IL7Ra+/KLRG1- of EGFR+
B.
Against CD19Lo Leukemia
C.
Against WT Leukemia
%CD27+/CD62L- of EGFR+
%CD27+/CD62L+ of EGFR+
D.
Against CD19Lo Leukemia
E.
Against WT Leukemia
%PD1+/TOX+ of EGFR+
F.
%PD1+/CD39+ of EGFR+
G.
Against CD19Lo Leukemia
H.
I.
% TCF1+/TIM3- of EGFR+
J.
% TCF1-/TIM3+ of EGFR+
K.
L.
CAR8MD
CAR8ND
EGFR8

Figure S5: Additional *in vivo* effector/memory and exhaustion phenotyping at low CAR dose (Related to Figure 3).

All data in this figure are from experiments with the 3e5 EGFR+ cell dose. **S5A:** Proportions of CAR8 with the short-lived effector cell (SLEC, IL7Ra-/KLRG1+) or memory precursor effector cell (MPEC, IL7Ra+/KLRG1-) phenotypes at the indicated timepoint against WT leukemia. **S5B:** Proportions of CAR8 with the short-lived effector cell (SLEC, IL7Ra-/KLRG1+) or memory precursor effector cell (MPEC, IL7Ra+/KLRG1-) phenotypes at the indicated timepoint against $CD19^{Lo}$ leukemia. **S5C:** Proportions of CAR8 with the effector memory precursor (EMP, CD27+/CD62L-) or central memory precursor (CMP, CD27+/CD62L+) phenotypes at the indicated timepoint against WT leukemia. **S5D:** Proportions of CAR8 with the effector memory precursor (EMP, CD27+/CD62L-) or central memory precursor (CMP, CD27+/CD62L+) phenotypes at the indicated timepoint against $CD19^{Lo}$ leukemia. Figures S4E-L display proportions of CAR8 with the indicated phenotype at 11 days post-CAR injection against either WT (left, E,F,I,J) or $CD19^{Lo}$ (right, G,H,K,L) leukemia. **S5E & G:** PD1+/TOX+ **S5F & H:** PD1+/CD39+ **S5I & K:** TCF1+/TIM3- **S5J & L:** TCF1-/TIM3+. Data are from 2 pooled, independent experiments with n=10 mice per condition. Data represent mean +/- SD. * $p<0.05$, ** $p<0.01$, *** $p<0.001$, **** $p<0.0001$.

Figure S6

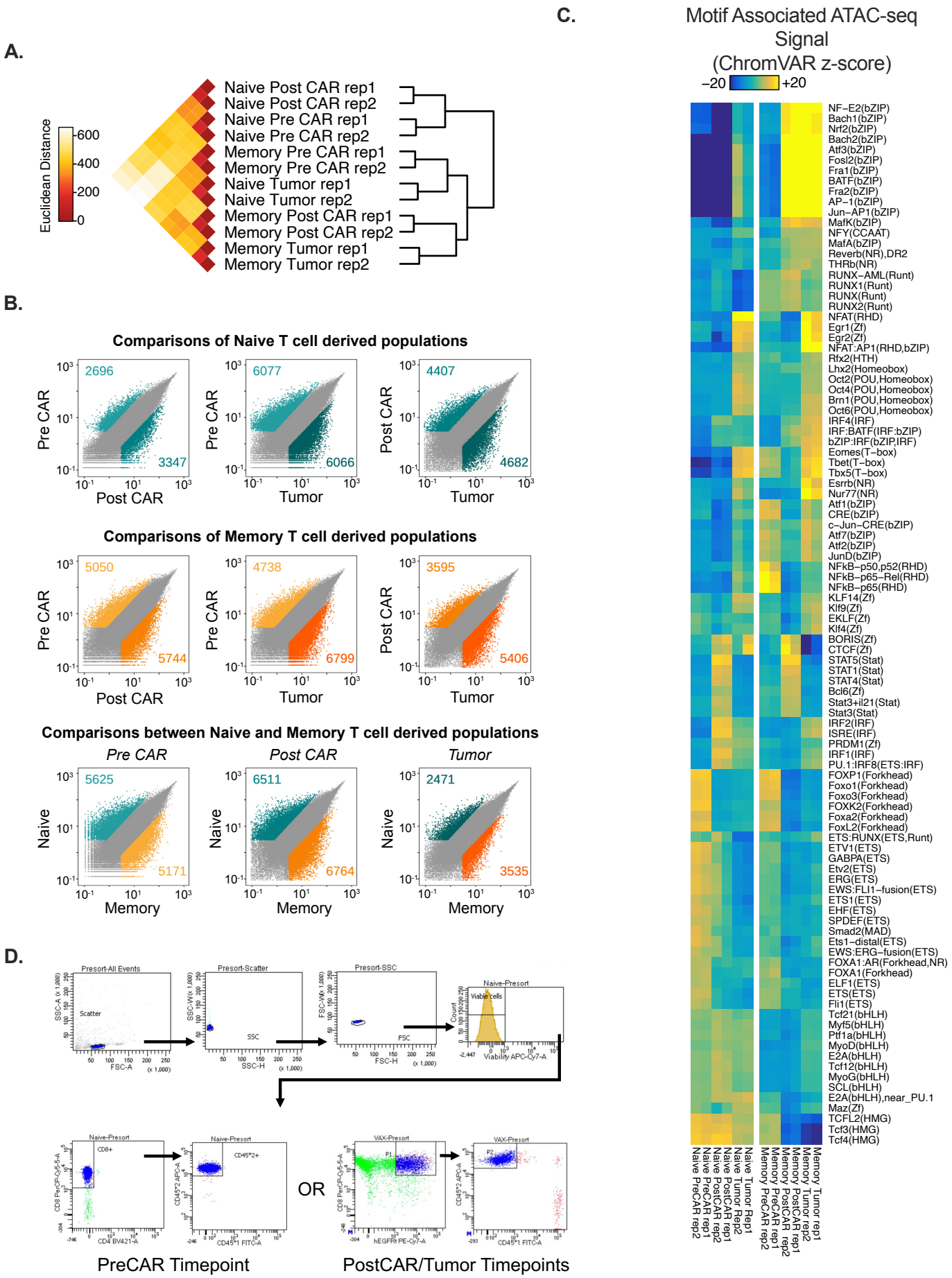
A.
Euclidean Distance
600
400
200
0
Naive Post CAR rep1
Naive Post CAR rep2
Naive Pre CAR rep1
Naive Pre CAR rep2
Memory Pre CAR rep1
Memory Pre CAR rep2
Naive Tumor rep1
Naive Tumor rep2
Memory Post CAR rep1
Memory Post CAR rep2
Memory Tumor rep1
Memory Tumor rep2
B.
Comparisons of Naive T cell derived populations
Pre CAR
Post CAR
2696
3347
6077
6066
Tumor
4407
4682
Comparisons of Memory T cell derived populations
5050
5744
4738
6799
3595
5406
Comparisons between Naive and Memory T cell derived populations
Pre CAR
Post CAR
Tumor
Naive
Memory
5625
5171
6511
6764
2471
3535
C.
Motif Associated ATAC-seq Signal (ChromVAR z-score)
−20
+20
NF−E2(bZIP)
Bach1(bZIP)
Nrf2(bZIP)
Bach2(bZIP)
Atf3(bZIP)
Fosl2(bZIP)
Fra1(bZIP)
BATF(bZIP)
Fra2(bZIP)
AP−1(bZIP)
Jun−AP1(bZIP)
MafK(bZIP)
NFY(CCAAT)
MafA(bZIP)
Reverb(NR),DR2
THRb(NR)
RUNX−AML(Runt)
RUNX1(Runt)
RUNX(Runt)
RUNX2(Runt)
NFAT(RHD)
Egr1(Zf)
Egr2(Zf)
NFAT:AP1(RHD,bZIP)
Rfx2(HTH)
Lhx2(Homeobox)
Oct2(POU,Homeobox)
Oct4(POU,Homeobox)
Brn1(POU,Homeobox)
Oct6(POU,Homeobox)
IRF4(IRF)
IRF:BATF(IRF:bZIP)
bZIP:IRF(bZIP,IRF)
Eomes(T−box)
Tbet(T−box)
Tbx5(T−box)
Esrrb(NR)
Nur77(NR)
Atf1(bZIP)
CRE(bZIP)
c−Jun−CRE(bZIP)
Atf7(bZIP)
Atf2(bZIP)
JunD(bZIP)
NFkB−p50,p52(RHD)
NFkB−p65−Rel(RHD)
NFkB−p65(RHD)
KLF14(Zf)
Klf9(Zf)
EKLF(Zf)
Klf4(Zf)
BORIS(Zf)
CTCF(Zf)
STAT5(Stat)
STAT1(Stat)
STAT4(Stat)
Bcl6(Zf)
Stat3+il21(Stat)
Stat3(Stat)
IRF2(IRF)
ISRE(IRF)
PRDM1(Zf)
IRF1(IRF)
PU.1:IRF8(ETS:IRF)
FOXP1(Forkhead)
Foxo1(Forkhead)
Foxo3(Forkhead)
FOXK2(Forkhead)
Foxa2(Forkhead)
FoxL2(Forkhead)
ETS:RUNX(ETS,Runt)
ETV1(ETS)
GABPA(ETS)
Etv2(ETS)
ERG(ETS)
EWS:FLI1−fusion(ETS)
ETS1(ETS)
EHF(ETS)
SPDEF(ETS)
Smad2(MAD)
Ets1−distal(ETS)
EWS:ERG−fusion(ETS)
FOXA1:AR(Forkhead,NR)
FOXA1(Forkhead)
ELF1(ETS)
ETS(ETS)
Fli1(ETS)
Tcf21(bHLH)
Myf5(bHLH)
Ptf1a(bHLH)
MyoD(bHLH)
E2A(bHLH)
Tcf12(bHLH)
MyoG(bHLH)
SCL(bHLH)
E2A(bHLH),near_PU.1
Maz(Zf)
TCFL2(HMG)
Tcf3(HMG)
Tcf4(HMG)
Naive PreCAR rep2
Naive PreCAR rep1
Naive PostCAR rep2
Naive PostCAR rep1
Naive Tumor Rep2
Naive Tumor Rep1
Memory PreCAR rep2
Memory PreCAR rep1
Memory PostCAR rep2
Memory PostCAR rep1
Memory Tumor rep2
Memory Tumor rep1
D.
Presort-All Events
Presort-Scatter
Presort-SSC
Naive-Presort
Viable cells
Scatter
SSC
FSC
Viability APC-Cy7-A
Naive-Presort
CD8+
CD45*2+
OR
VAX-Presort
P1
P2
PreCAR Timepoint
PostCAR/Tumor Timepoints

Figure S6: Additional analyses of ATAC-seq data (Related to Figure 4).

All analyses in this figure are from the same timeline/experimental layout described in Figure 4A. **S6A:** Inter-replicate Euclidian distance of voom-normalized ATAC-seq counts per peak between biological replicates. **S6B:** Pairwise comparisons of differentially accessible chromatin regions within conditions between different timepoints of the same condition, or between different conditions at each timepoint. Data points are mean of voom-normalized ATAC-seq counts per peak between biological replicates of each group. **S6C:** Heatmap of motif-associated ChromVAR deviation z-scores patterns of motif-associated ATAC-seq signal for indicated transcription factors. List comprises all significant differentially accessible comparisons. **S6D:** Representative gating for sorting of cells in sequencing experiments.

Figure S7

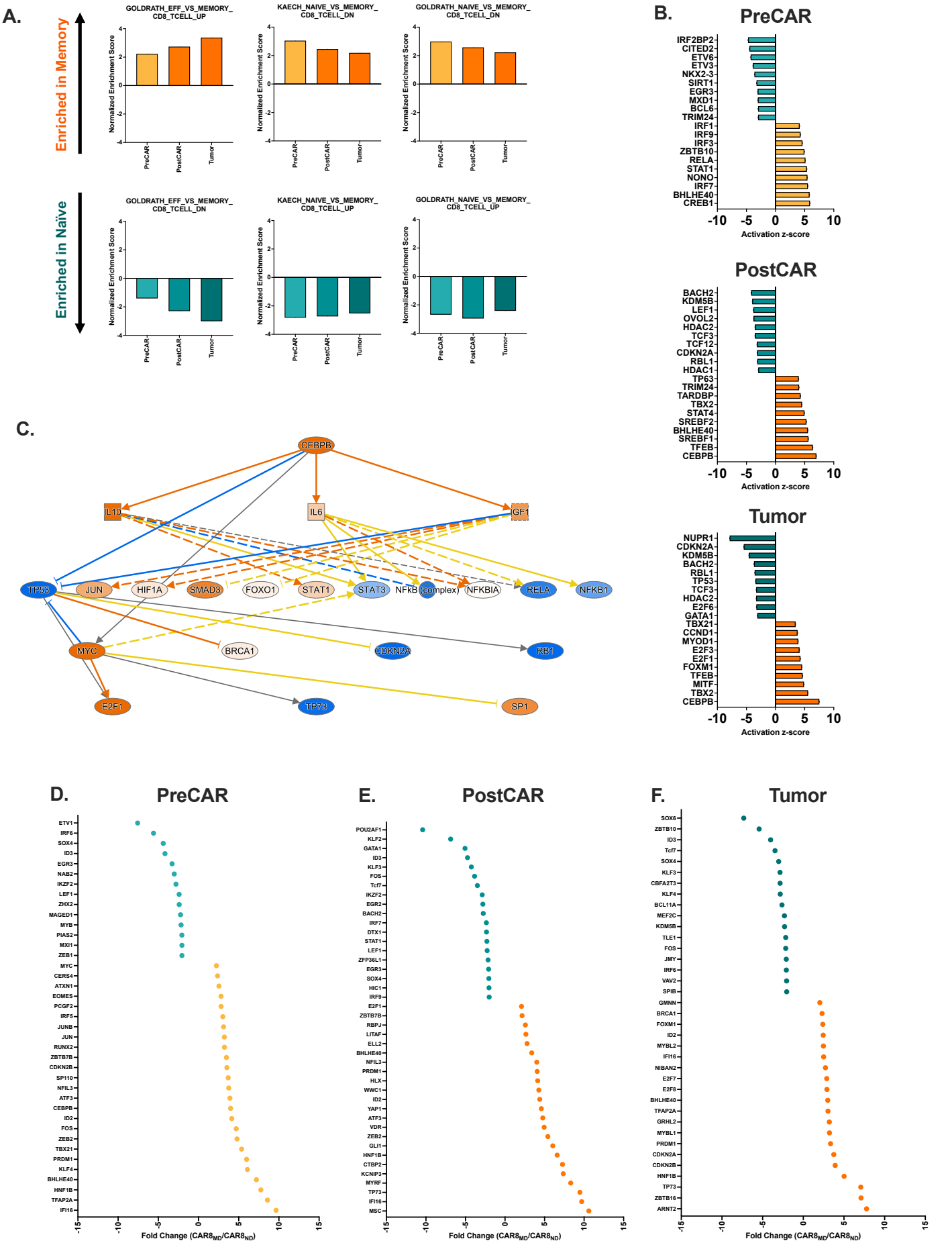
A.
Enriched in Memory
Enriched in Naïve
GOLDRATH_EFF_VS_MEMORY_CD8_TCELL_UP
KAECH_NAIVE_VS_MEMORY_CD8_TCELL_DN
GOLDRATH_NAIVE_VS_MEMORY_CD8_TCELL_DN
GOLDRATH_EFF_VS_MEMORY_CD8_TCELL_DN
KAECH_NAIVE_VS_MEMORY_CD8_TCELL_UP
GOLDRATH_NAIVE_VS_MEMORY_CD8_TCELL_UP
Normalized Enrichment Score
PreCAR
PostCAR
Tumor
B.
PreCAR
IRF2BP2
CITED2
ETV6
ETV3
NKX2-3
SIRT1
EGR3
MXD1
BCL6
TRIM24
IRF1
IRF9
IRF3
ZBTB10
RELA
STAT1
NONO
IRF7
BHLHE40
CREB1
PostCAR
BACH2
KDM5B
LEF1
OVOL2
HDAC2
TCF3
TCF12
CDKN2A
RBL1
HDAC1
TP63
TRIM24
TARDBP
TBX2
STAT4
SREBF2
BHLHE40
SREBF1
TFEB
CEBPB
Tumor
NUPR1
CDKN2A
KDM5B
BACH2
RBL1
TP53
TCF3
HDAC2
E2F6
GATA1
TBX21
CCND1
MYOD1
E2F3
E2F1
FOXM1
TFEB
MITF
TBX2
CEBPB
-10 -5 0 5 10
Activation z-score
C.
CEBPB
IL10
IL6
GF1
TP53
JUN
HIF1A
SMAD3
FOXO1
STAT1
STAT3
NFKB (complex)
NFKBIA
RELA
NFKB1
MYC
BRCA1
CDKN2A
RB1
E2F1
TP73
SP1
D.
PreCAR
ETV1
IRF6
SOX4
ID3
EGR3
NAB2
IKZF2
LEF1
ZHX2
MAGED1
MYB
PIAS2
MXI1
ZEB1
MYC
CERS4
ATXN1
EOMES
PCGF2
IRF5
JUNB
JUN
RUNX2
ZBTB7B
CDKN2B
SP110
NFIL3
ATF3
CEBPB
ID2
FOS
ZEB2
TBX21
PRDM1
KLF4
BHLHE40
HNF1B
TFAP2A
IFI16
-15 -10 -5 0 5 10 15
Fold Change (CAR8MD/CAR8ND)
E.
PostCAR
POU2AF1
KLF2
GATA1
ID3
KLF3
FOS
Tcf7
IKZF2
EGR2
BACH2
IRF7
DTX1
STAT1
LEF1
ZFP36L1
EGR3
SOX4
HIC1
IRF9
E2F1
ZBTB7B
RBPJ
LITAF
ELL2
BHLHE40
NFIL3
PRDM1
HLX
WWC1
ID2
YAP1
ATF3
VDR
ZEB2
GLI1
HNF1B
CTBP2
KCNIP3
MYRF
TP73
IFI16
MSC
-15 -10 -5 0 5 10 15
Fold Change (CAR8MD/CAR8ND)
F.
Tumor
SOX6
ZBTB10
ID3
Tcf7
SOX4
KLF3
CBFA2T3
KLF4
BCL11A
MEF2C
KDM5B
TLE1
FOS
JMY
IRF6
VAV2
SPIB
GMNN
BRCA1
FOXM1
ID2
MYBL2
IFI16
NIBAN2
E2F7
E2F8
BHLHE40
TFAP2A
GRHL2
MYBL1
PRDM1
CDKN2A
CDKN2B
HNF1B
TP73
ZBTB16
ARNT2
-15 -10 -5 0 5 10 15
Fold Change (CAR8MD/CAR8ND)

Figure S7: Additional analyses of RNA-seq data (Related to Figure 5).

All analyses in this figure are from the same timeline/experimental layout described in Figure 4A. **S7A:** Normalized enrichment scores from GSEA of differentially enriched genesets between indicated CD8+ T cell subsets after LCMV-armstrong acute viral infection[24, 25]. **S7B:** Top transcriptional activators predicted to be activated and driving differential transcriptional state between naïve versus memory-derived cells at the indicated timepoint, as predicted by Qiagen Ingenuity Pathway Analysis[28] (IPA). **S7C:** IPA activation map for the Cebpb transcription factor, the top predicted driver of transcriptional state in memory-derived cells at the PostCAR and Tumor timepoints. **S7D-F:** Top differentially expressed transcription factors, at the indicated timepoint. All statistics performed using DESeq2 with filtering threshold at 10, log2foldchange >2 and padj > 0.05.

Figure S8

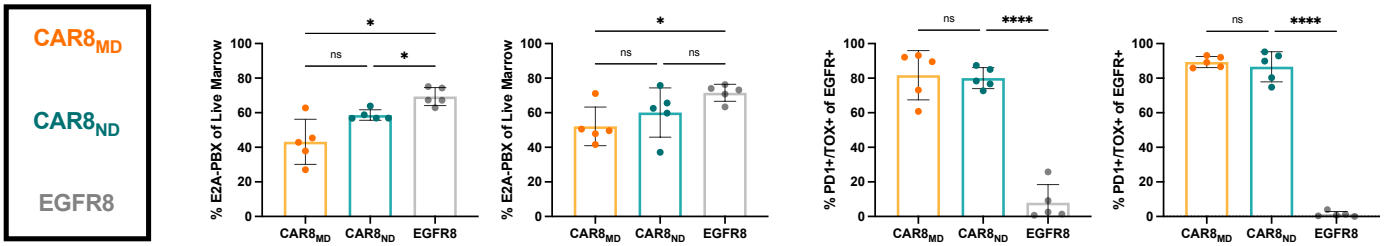
CAR8MD
CAR8ND
EGFR8
A.
Against WT Leukemia
Against CD19Lo Leukemia
% E2A-PBX of Live Marrow
B.
% PD1+/TOX+ of EGFR+
ns
*
****

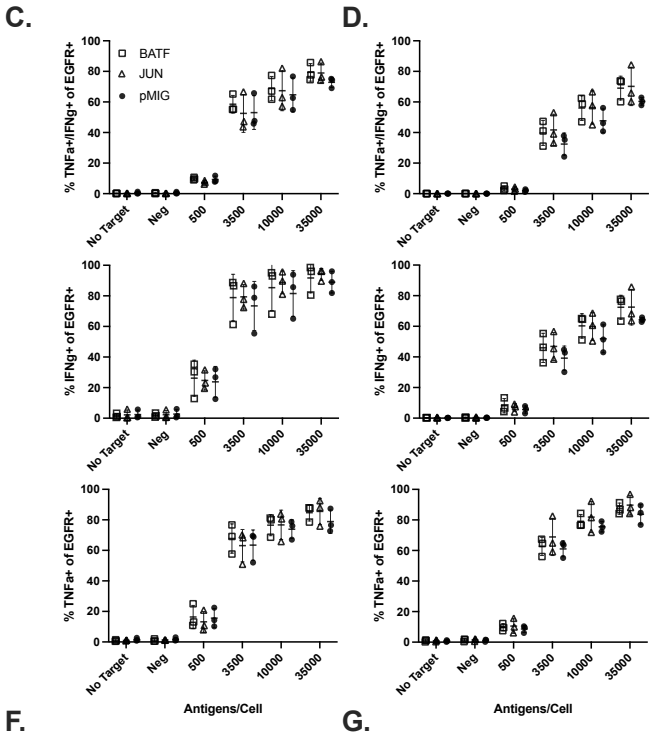
C.
D.
BATF
JUN
pMIG
% TNFa+/IFNg+ of EGFR+
% IFNg+ of EGFR+
% TNFa+ of EGFR+
No Target
Neg
500
3500
10000
35000
Antigens/Cell

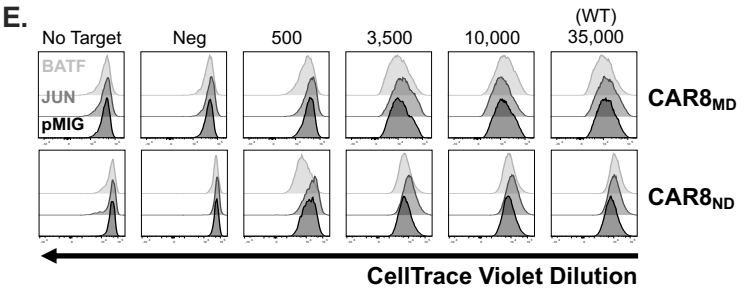
E.
No Target
Neg
500
3,500
10,000
(WT)
35,000
BATF
JUN
pMIG
CAR8MD
CAR8ND
CellTrace Violet Dilution

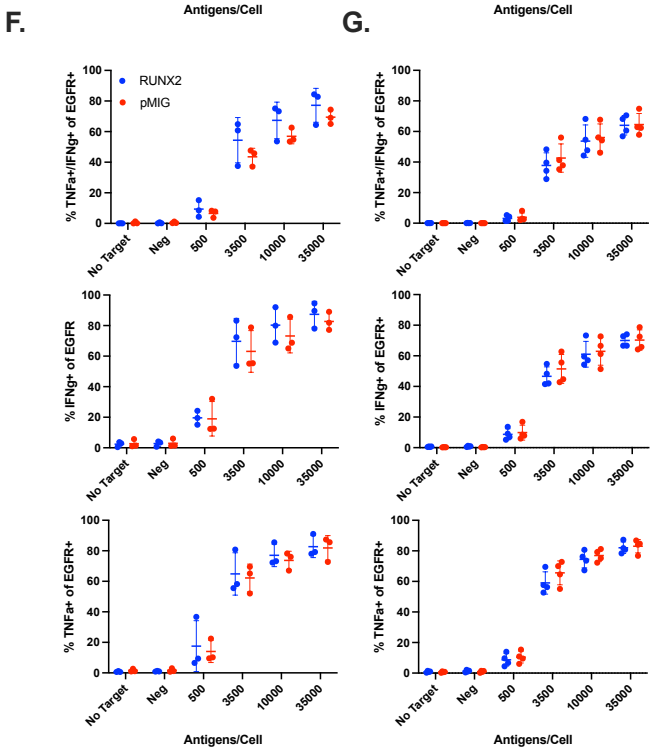
F.
G.
RUNX2
pMIG
% TNFa+/IFNg+ of EGFR+
% IFNg+ of EGFR
% TNFa+ of EGFR+
No Target
Neg
500
3500
10000
35000
Antigens/Cell

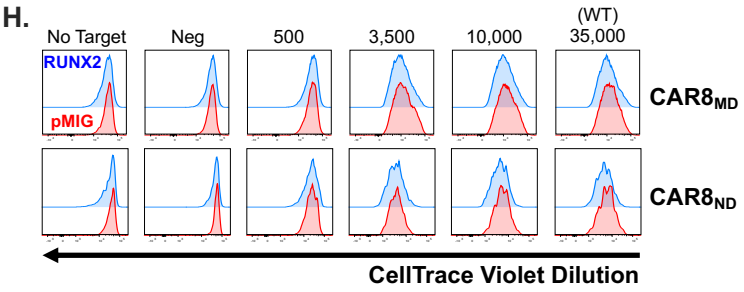
H.
No Target
Neg
500
3,500
10,000
(WT)
35,000
RUNX2
pMIG
CAR8MD
CAR8ND
CellTrace Violet Dilution

Figure S8 (Related to Figure 6): Characterization of 1e5 CAR T cell dose *in vivo* experiments and *in vitro* comparisons of BATF, JUN or RUNX2 overexpressing cells to pMIG.

All analyses in this figure are the same timeline/experimental layout described in Figure 3A except with 1e5 CAR+ cell dose, at 11 days post-CAR timepoint. S8A-B are characterization of the 1e5 cell dose with standard T cell groups (no ectopic transcription factor expression). **S8A:** Leukemia burden. **S8B:** Proportions of CAR8 with the PD1+/TOX+ phenotype. Data in S7A-B are from 1 experiment with n=5 mice per condition. * $p<0.05$, ** $p<0.01$, *** $p<0.001$, **** $p<0.0001$. **S8C-D:** Quantification of intracellular cytokine staining of IFNg and TNFa after 6 hour co-culture assay, % positive of EGFR+, for memory (C) or naïve-derived (D) cells cotransduced with BATF, JUN or pMIG. Data in S8C-D are from 3 independent experiments. **S8E:** Proliferation as measured by dilution of CellTrace Violet dye dilution of EGFR+ cells after 72 hour co-culture assay, for memory or naïve derived cells cotransduced with BATF, JUN or pMIG. Data representative of 3 independent experiments. **S8F-G:** Quantification of intracellular cytokine staining of IFNg and TNFa after 6 hour co-culture assay, % positive of EGFR+, for memory (C) or naïve-derived (D) cells cotransduced with RUNX2 or pMIG. Data in S8C-D are from 3-4 independent experiments. **S8H:** Proliferation as measured by dilution of CellTrace Violet dye dilution of EGFR+ cells after 72 hour co-culture assay, for memory or naïve derived cells cotransduced with RUNX2 or pMIG. Data representative of 3 independent experiments. No statistically significant differences were found between BATF, JUN or RUNX2 engineered CAR T cells and pMIG control T cells for in vitro data. Data represent mean +/- SD.

Figure S9

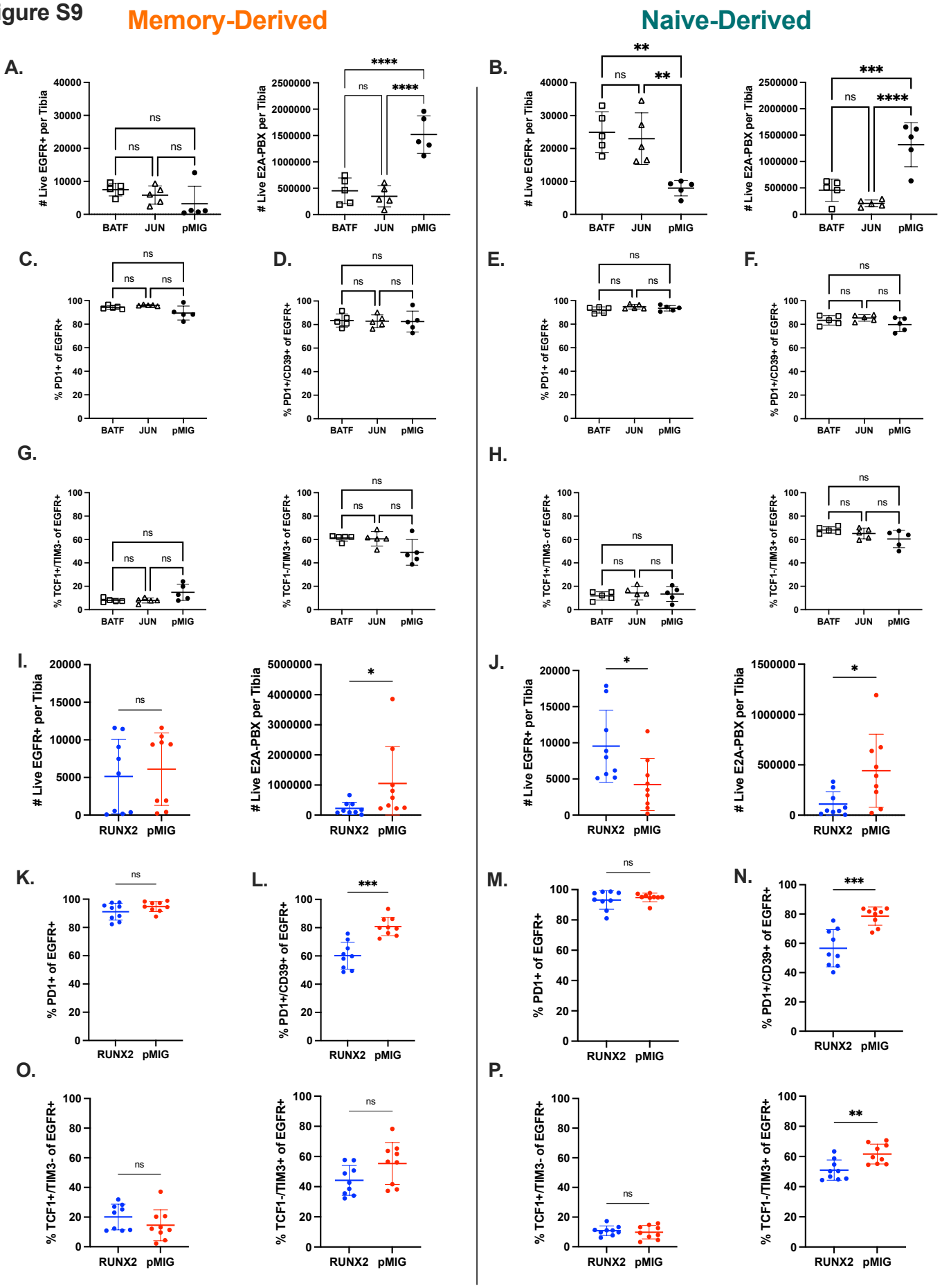
Memory-Derived
Naive-Derived
A.
B.
C.
D.
E.
F.
G.
H.
I.
J.
K.
L.
M.
N.
O.
P.
Live EGFR+ per Tibia
Live E2A-PBX per Tibia
% PD1+ of EGFR+
% PD1+/CD39+ of EGFR+
% TCF1+/TIM3- of EGFR+
% TCF1-/TIM3+ of EGFR+
BATF
JUN
pMIG
RUNX2
pMIG
ns
*
**
***
****

Figure S9 (Related to Figure 6): Counts and additional exhaustion phenotyping data for BATF, JUN or RUNX2 overexpression *in vivo* experiments.

All analyses in this figure are done on the same experiments described in Figure 6. Counts data was generated by flushing a single tibia and using total tibia counts and cytometer proportions data to calculate CAR and leukemia cell counts per tibia. **S9A-B:** CAR and leukemia counts for BATF or JUN overexpressing memory (A) or naïve-derived (B) CAR T cells compared to pMIG control. **S9C-H:** Proportions of EGFR+ cells from BATF, JUN or pMIG CAR8 with the indicated phenotype. S9C,D,G are memory-derived cells, S9E,F,H are naïve-derived cells. **S9C,E:** PD1+ **S9D,F:** PD1+/CD39+ **S9G-H:** Indicated TCF1/TIM3 phenotype. Data in S9A-H are from one experiment with n=5 mice per condition. **S9I-J:** CAR and leukemia counts for RUNX2 overexpressing memory (A) or naïve-derived (B) CAR T cells compared to pMIG control. **S9K-N:** Proportions of EGFR+ cells from RUNX2 or pMIG CAR8 with the indicated phenotype. S9C,D,G are memory-derived cells, S9E,F,H are naïve-derived cells. **S9K,M:** PD1+ **S9L,N:** PD1+/CD39+ **S9O,P:** Indicated TCF1/TIM3 phenotype. Data in S9I-P are from 2 pooled, independent experiments with n=9 mice per condition. Data represent mean +/- SD. * $p<0.05$, ** $p<0.01$, *** $p<0.001$, **** $p<0.0001$.